A crystallographic non-centrosymmetric versus centrosymmetric study by electron diffraction on the melt-grown Sr- and O-deficient n = 5 type Carpy-Galy phase Sr17CaBaNb19WO64 of the Schückel-Müller-Buschbaum type which is potentially a polar or ferroelectric quasi-1D metal

Report

Author(s):
Lichtenberg, Frank; Baghi Zadeh, Ali; Zaubitzer, Christian; Grafulha Morales, Luiz; Simonov, Arkadiy

Publication date:
2024-06-28

Permanent link:
https://doi.org/10.3929/ethz-b-000680533

Published in 2024 by the library of the ETH Zurich via doi 10.3929/ethz-b-000680533

A crystallographic non-centrosymmetric versus centrosymmetric study by electron diffraction on the melt-grown Sr- and O-deficient n = 5 type Carpy-Galy phase $Sr_{17}CaBaNb_{19}WO_{64}$ of the Schückel-Müller-Buschbaum type which is potentially a polar or ferroelectric quasi-1D metal

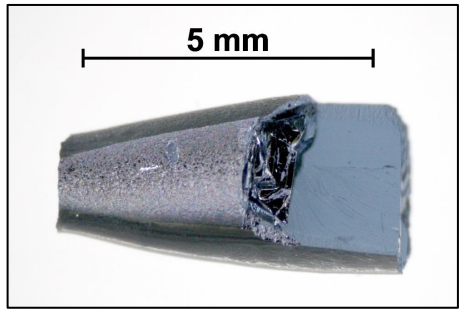

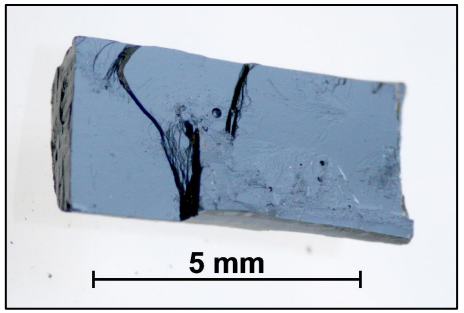

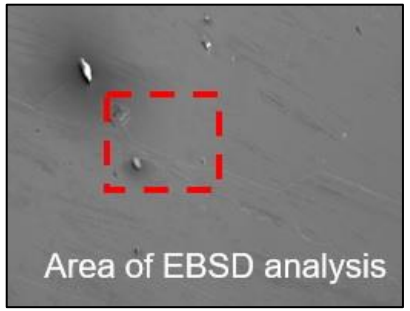

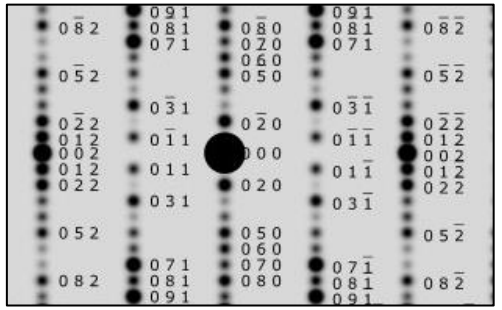

Frank Lichtenberg [1] , Ali Baghi Zadeh [2] , Christian Zaubitzer [2] , Luiz Grafulha Morales [2] , and Arkadiy Simonov [3]

ETH Zurich, 8093 Zurich, Switzerland

[1] Department of Materials, Division of Prof. Nicola Spaldin, https://theory.mat.ethz.ch/lab.html

[2] Scientific Center for Optical and Electron Microscopy (ScopeM), https://scopem.ethz.ch

[3] Department of Materials, Disorder group, https://ferroic.mat.ethz.ch/the-group/disorder.html

28 June 2024

This paper in form of a presentation comprises 45 pages, a content overview, an introduction and summary, and many images. It is published by the library of the ETH Zurich / ETH Research Collection via
doi 10.3929/ethz-b-000680533:

https://doi.org/10.3929/ethz-b-000680533

It allows the download of this paper as pdf presentation.

1 Introduction & Summary ...

In a paper from 1985 K. Schückel and Hk. Müller-Buschbaum report about the reduced and mixed valence niobate $Sr_5Nb_5O_{16}$ [1]. Small amounts of small crystals were obtained by a special technique which comprises the use of a H_2 / H plasma. The crystals were studied by single crystal x-ray diffraction and energy-dispersive x-ray spectroscopy. The crystal structure of $Sr_5Nb_5O_{16}$ is perovskite-related, layered, orthorhombic, and non-centrosymmetric. Physical properties are not reported.

In a paper from 2008 F. Lichtenberg et al. present the realization that $Sr_5Nb_5O_{16} \triangleq SrNbO_{3.2}$ represents an oxygen-deficient variant of $Sr_5Nb_5O_{17} \triangleq SrNbO_{3.4}$ with fully ordered oxygen vacancies [2]. The crystal structure of $Sr_5Nb_5O_{17} \triangleq SrNbO_{3.4}$ is perovskite-related, layered, orthorhombic, and centrosymmetric [3].
$Sr_5Nb_5O_{17} \triangleq SrNbO_{3.4}$ is an $n = 5$ type member of the homologous series $A_nB_nO_{3n+2} \triangleq ABO_x$ and a quasi-1D metal, see Refs. [2 – 5] and references therein.

$A_nB_nO_{3n+2} \triangleq ABO_x$ represent a homologous series of perovskite-related layered oxides and are meanwhile called Carpy-Galy phases. The layers comprise an arrangement of BO_6 octahedra which are $[110]_{perovskite}$ oriented along the *c*-axis.

The index or structure type n describes the thickness of the layers which are n BO_6 octahedra thick along the c-axis. For $n = \infty$ the non-layered perovskite structure ABO_3 is obtained.
A sketch of their crystal structure and compositional examples are presented on pages 10 - 15.

The following items are examples why oxides of the type $A_nB_nO_{3n+2} \triangleq ABO_x$ are interesting, see Refs. [2 – 8] and references therein:

- In contrast to most layered materials they display a pronounced structural anisotropy also within the layers which extend along the ab-plane
- They comprise the highest-T_c ferroelectrics such as the n = 4 type $La_4Ti_4O_{14} \triangleq La_2Ti_2O_7 \triangleq LaTiO_{3.5}$ with T_c = 1770 K
- They comprise quasi-1D metals in which the delocalized electrons are embedded in a ferroelectric-like environment such as the n = 5 type $Sr_5Nb_5O_{17} \triangleq SrNbO_{3.4}$ and some of the quasi-1D metals are most probably polar or ferroelectric quasi-1D metals
- Many compounds can be synthesized in a single phase and crystalline form via a solidification from the melt by using the floating zone technique
- They might have a potential to create superconductors and / or multiferroics

- There are many possible chemical compositions including non-stoichiometric compounds
- The quasi-1D metals $SrNbO_{3.45}$ (n = 4.5) and Sr- and O-deficient $Sr_{0.95}NbO_{3.37}$ (n = 5) were studied by special optical techniques which revealed the presence of photoinduced metastable dd-exciton-driven metal-to-insulator transitions
- The Sr- and O-deficient n = 5 type qausi-1D metal $Sr_{0.95}NbO_{3.37}$ was studied by resonant soft x-ray scattering which revealed the presence of two distinct and simultaneous charge density waves along the non-metallic c-axis

The already mentioned $Sr_{20}Nb_{20}O_{68} \triangleq Sr_5Nb_5O_{17} \triangleq SrNbO_{3.4}$ and $Sr_{20}Nb_{20}O_{64} \triangleq Sr_5Nb_5O_{16} \triangleq SrNbO_{3.2}$ represent another interesting topic and associated comments and open questions are presented on pages 225 – 227 in part 6.7 of Ref. [5]. The quasi-1D metal $Sr_5Nb_5O_{17} \triangleq SrNbO_{3.4}$ can be prepared via the melt by using the floating zone technique but attempts to prepare $Sr_5Nb_5O_{16} \triangleq SrNbO_{3.2}$ in the same way were not successful [2, 5]. Meanwhile, however, the synthesis of related materials in a single phase and crystalline form via the melt by using the floating zone technique is reported in a paper from 2020, namely $Sr_{17}CaBaNb_{19}WO_{64}$ and $Sr_{17}Ca_2Nb_{19}WO_{64}$ [5]. They are called Sr- and O-deficient n = 5 type Carpy-Galy phases of the Schückel-Müller-Buschbaum type.

The availability of melt-grown $Sr_{17}CaBaNb_{19}WO_{64}$ and $Sr_{17}Ca_2Nb_{19}WO_{64}$ leads to several comments and open questions which are presented in part 6.9.8 of Ref. [5]. The topic of this work is $Sr_{17}CaBaNb_{19}WO_{64}$ and here we present from Ref. [5] some pictures of the melt-grown material:

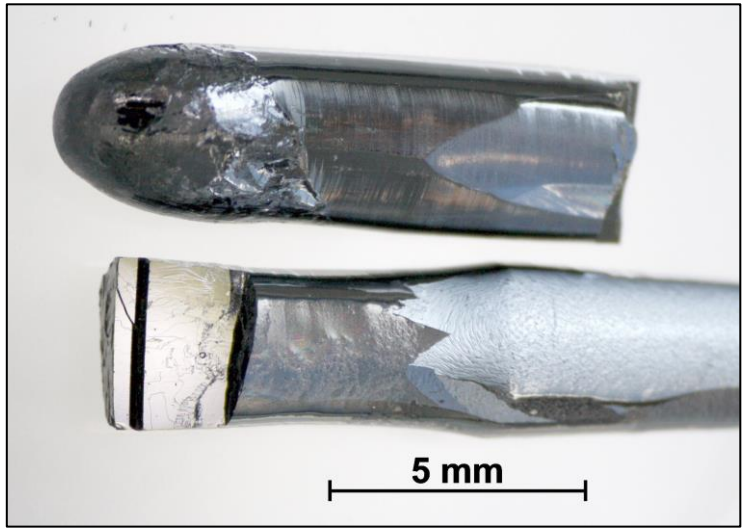

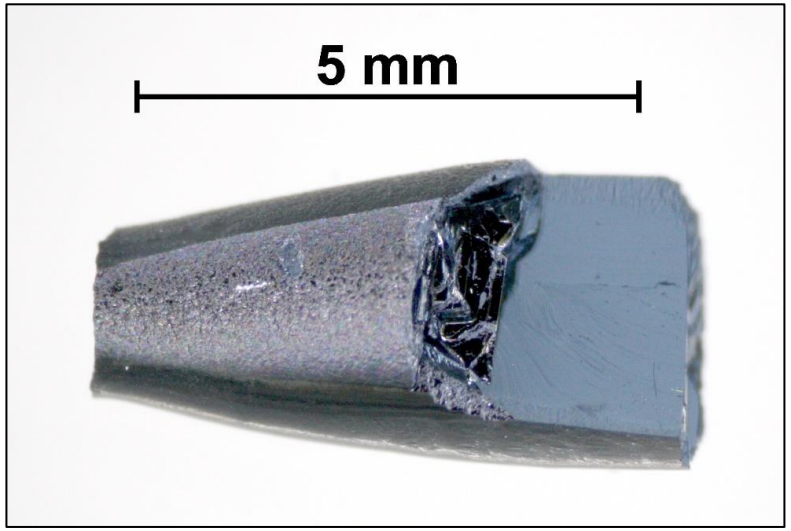

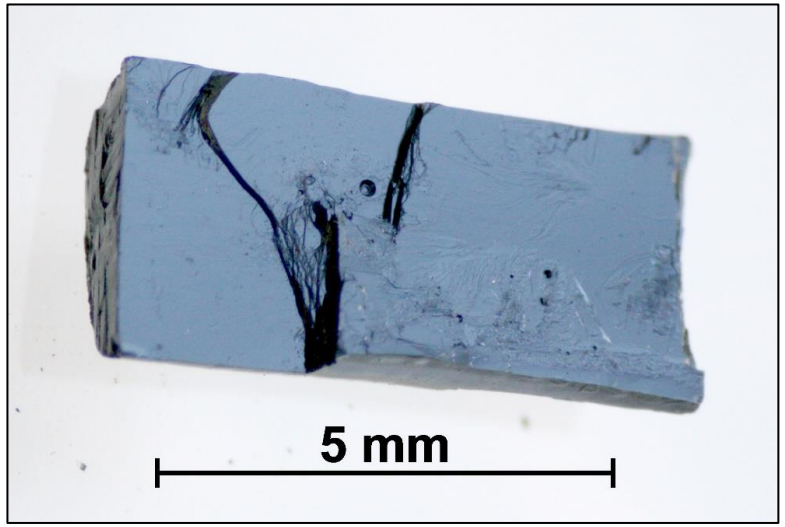

The magnetic susceptibility $\chi(T)$ of melt-grown $Sr_{17}CaBaNb_{19}WO_{64}$ and $Sr_{17}Ca_2Nb_{19}WO_{64}$ indicates that they are quasi-1D metals like $Sr_{20}Nb_{20}O_{68}$ [5]. The reported non-centrosymmetric space group for $Sr_{20}Nb_{20}O_{64} \triangleq Sr_5Nb_5O_{16}$ [1] suggests that $Sr_{17}CaBaNb_{19}WO_{64}$ and $Sr_{17}Ca_2Nb_{19}WO_{64}$ are likewise non-centrosymmetric.

If a non-centrosymmetric crystal structure can be experimentally confirmed, then $Sr_{17}CaBaNb_{19}WO_{64}$ and $Sr_{17}Ca_2Nb_{19}WO_{64}$ are most probably polar or ferroelectric quasi-1D metals. $Sr_{17}CaBaNb_{19}WO_{64}$ was studied with respect to the question if its crystal structure is non-centrosymmetric or centrosymmetric and this paper presents the results.

The following pages 10 – 14 present some sketches of the crystal structure of Carpy-Galy phases $A_nB_nO_{3n+2} \triangleq ABO_x$, compositional examples from the system $SrNbO_x$, and sketches of the crystal structure of $Sr_{20}Nb_{20}O_{68} \triangleq Sr_5Nb_5O_{17} \triangleq SrNbO_{3.4}$ and $Sr_{20}Nb_{20}O_{64} \triangleq Sr_5Nb_5O_{16} \triangleq SrNbO_{3.2}$

Sketch of the perovskite-related layered structure of $A_nB_nO_{3n+2} \triangleq ABO_x$

☒ = BO_6 octahedra (O located at corners, *B* hidden in center)

B – O and BO_6 chains along a-axis, i.e. ⊥ drawing plane

b

c II [110]$_{perovskite}$

For Refs. see [2 - 5] and references therein

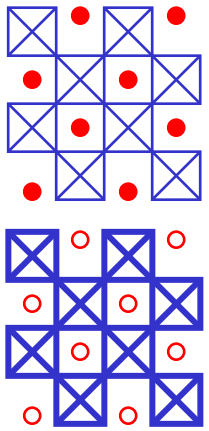

n = 4

$ABO_{3.5}$

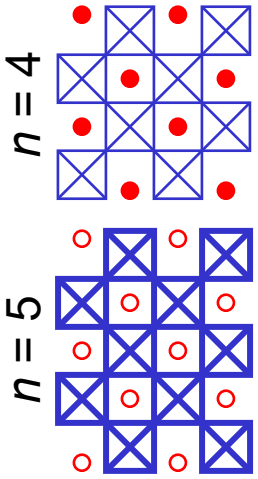

n = 4.5

$ABO_{3.44}$

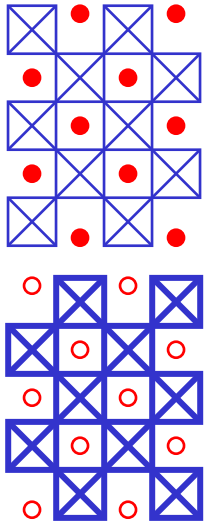

n = 5 (I)

$ABO_{3.4}$

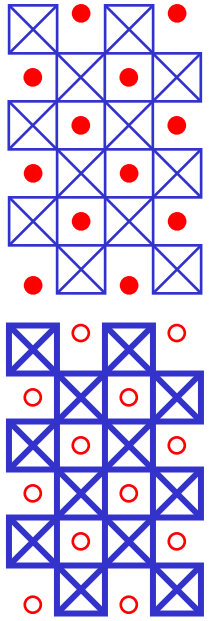

n = 6

$ABO_{3.33}$

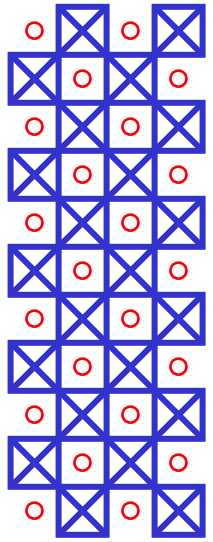

n = ∞

ABO_3 perovskite

Light and heavy drawing of the BO_6 octahedra as well as filled and open circles indicate a height difference perpendicular to the drawing plane

Sketch of the perovskite-related layered structure of $A_nB_nO_{3n+2} \triangleq ABO_x$

⊠ = BO_6 octahedra (O located at corners, *B* hidden in center)

⊡ = BO_4 polyhedra (O located at corners, *B* in the center)

B – O and BO_6 chains along a-axis, i.e. ⊥ drawing plane

b

c II [110]$_{perovskite}$

For Refs. see [1 - 5] and references therein

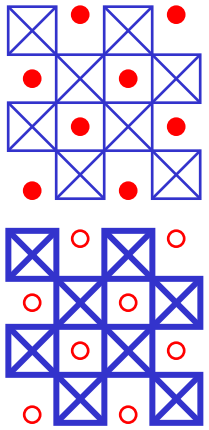

n = 4

$ABO_{3.5}$

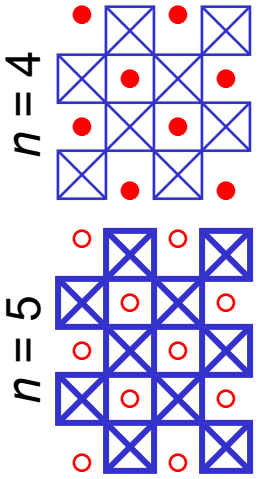

Ordered stacking sequence
n = 5 , 4 , 5 , 4 ...

n = 4.5

$ABO_{3.44}$

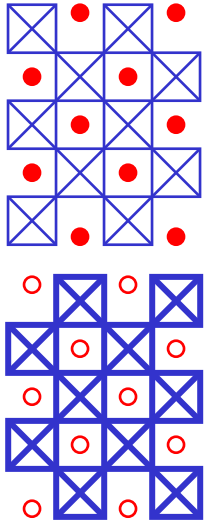

n = 5 (I)

$ABO_{3.4}$

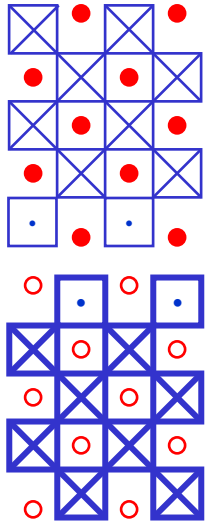

n = 5 (II)

$ABO_{3.2}$

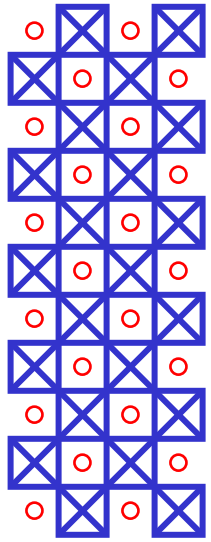

n = ∞

ABO_3 perovskite

Light and heavy drawing of the BO_6 octahedra and BO_4 polyhedra as well as filled and open circles indicate a height difference perpendi-cular to the drawing plane

Sketch of the perovskite-related layered structure of $A_nB_nO_{3n+2} \triangleq ABO_x$

☒ = BO_6 octahedra (O located at corners, *B* hidden in center)

⊡ = BO_4 polyhedra (O located at corners, *B* in the center)

B – O and BO_6 chains along a-axis, i.e. ⊥ drawing plane

Compositional examples from the system $SrNbO_x$ with Nb^{5+} ($4d^0$) and / or Nb^{4+} ($4d^1$)

For Refs. see [1 - 5] and references therein

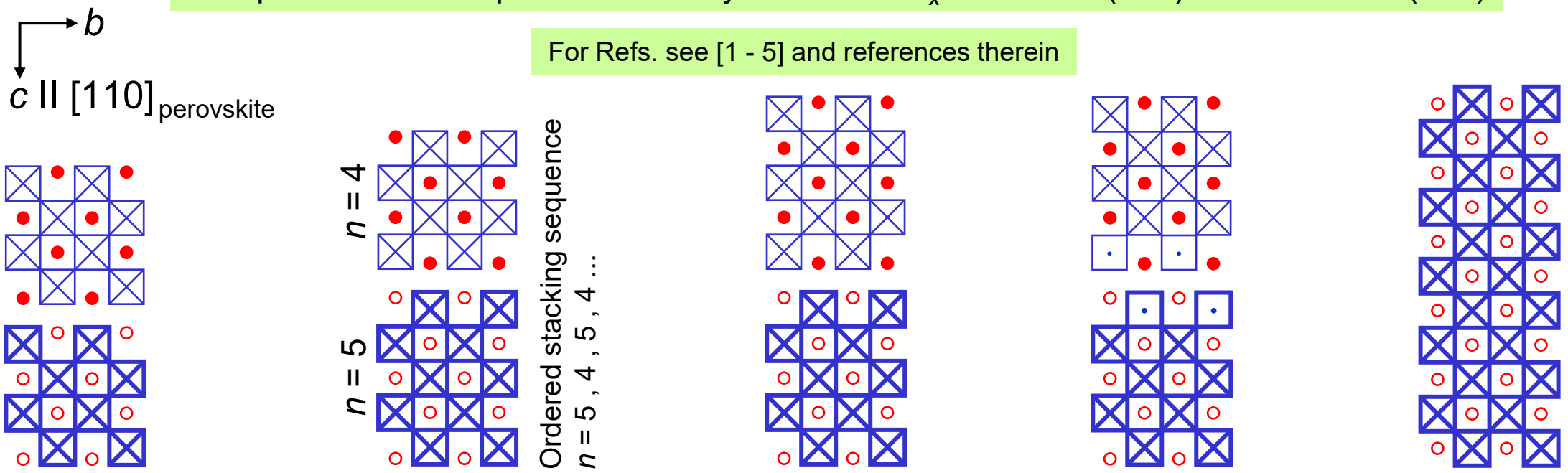

Light and heavy drawing of the BO_6 octahedra and BO_4 polyhedra as well as filled and open circles indicate a height difference perpendicular to the drawing plane

n = 4	*n* = 4.5	*n* = 5 (I)	*n* = 5 (II)	*n* = ∞
$ABO_{3.5}$	$ABO_{3.44}$	$ABO_{3.4}$	$ABO_{3.2}$	ABO_3 perovskite
$SrNbO_{3.5}$	$SrNbO_{3.44}$	$SrNbO_{3.4}$	$SrNbO_{3.2}$	$SrNbO_3$
non-centrosym. ferroelectric	centrosymmetric quasi-1D metal	centrosymmetric quasi-1D metal	non-centrosym. quasi-1D metal ?	centrosym. metal

The crystal structure of the n = 5 (II) type $Sr_{20}Nb_{20}O_{64}$ and the n = 5 (I) type $Sr_{20}Nb_{20}O_{68}$

= NbO_6 octahedra (O located at the corners, Nb hidden in the center)

= NbO_4 (O located at the corners, Nb in the center) = Sr

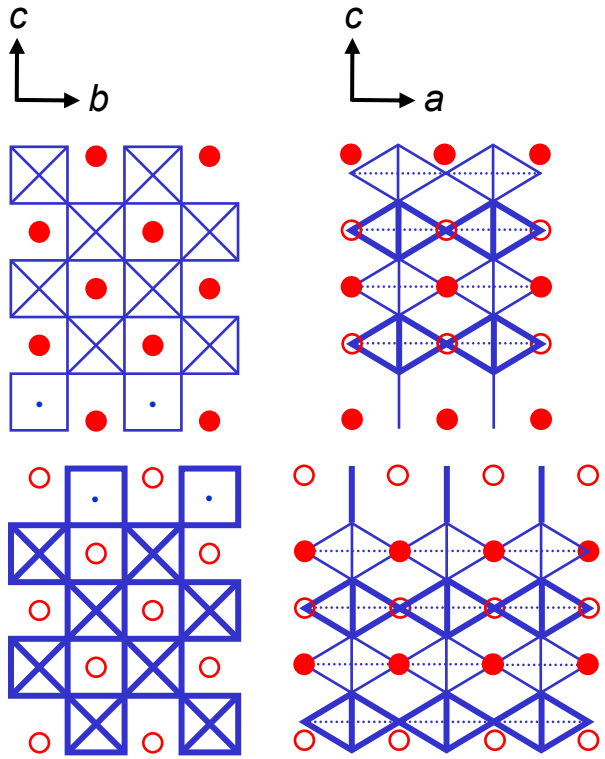

Nb – O polyhedra distortion in percent

25	Nb^{5+}	Nb^{5+}	23
21	Nb^{5+}	Nb^{5+}	17
20	Nb^{4+}	Nb^{4+}	3
9	Nb^{4+}	Nb^{5+}	17
36	Nb^{4+}	Nb^{5+}	23
36	Nb^{4+}	Nb^{5+}	23
9	Nb^{4+}	Nb^{5+}	17
20	Nb^{4+}	Nb^{4+}	3
21	Nb^{5+}	Nb^{5+}	17
25	Nb^{5+}	Nb^{5+}	23

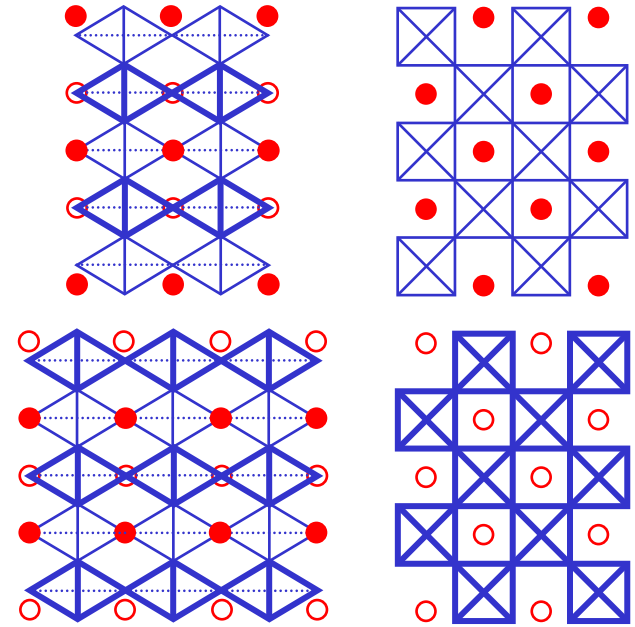

Light and heavy drawing of the BO_6 octahedra and BO_4 polyhedra as well as filled and open circles indicate a height difference perpendicular to the drawing plane

$SrNbO_{3.2} \triangleq Sr_5Nb_5O_{16} \triangleq Sr_{20}Nb_{20}O_{64}$
Non-centrosymmetric ! • Space Group No 31
Probably also a quasi-1D metal

K. Schückel and Hk. Müller-Buschbaum
Z. Anorg. Allg. Chem. 528 (1985) 91

Nb^{5+} / $4d^0$
Nb^{4+} / $4d^1$

F. Lichtenberg et al., Progress in Solid State Chem. 36 (2008) 253

$SrNbO_{3.4} \triangleq Sr_5Nb_5O_{17} \triangleq Sr_{20}Nb_{20}O_{68}$
Centrosymmetric • Space group No. 58
Quasi-1D metal

S. C. Abrahams et al.
Acta Cryst. B 54 (1998) 399

The crystal structure of the $n = 5$ (II) type $Sr_{20}Nb_{20}O_{64}$ and the $n = 5$ (I) type $Sr_{20}Nb_{20}O_{68}$

= NbO_6 octahedra (O located at the corners, Nb hidden in the center)

= NbO_4 (O located at the corners, Nb in the center)

(Fully ordered) oxygen vacancies are located at opposite boundaries of the layers or slabs

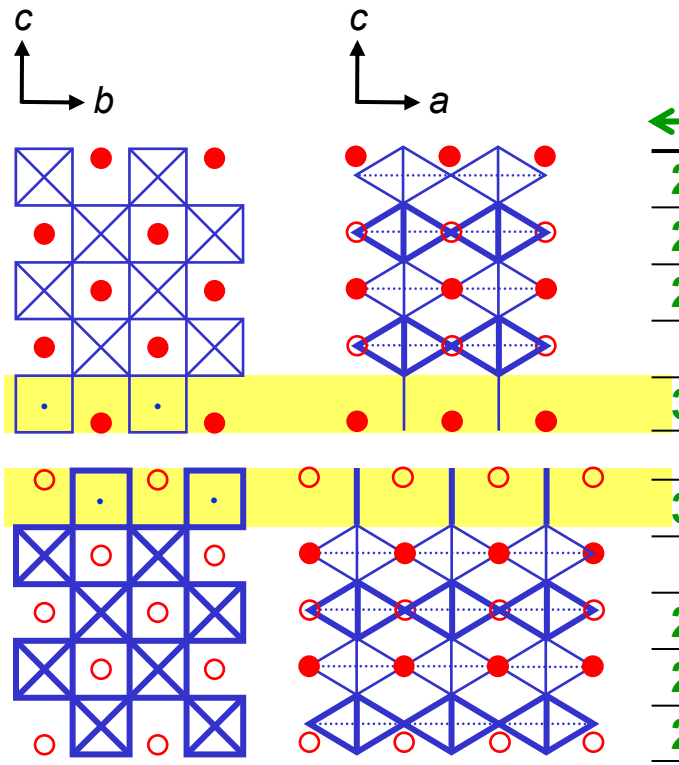

Nb – O polyhedra distortion in percent

25	Nb^{5+}	Nb^{5+}	23
21	Nb^{5+}	Nb^{5+}	17
20	Nb^{4+}	Nb^{4+}	3
9	Nb^{4+}	Nb^{5+}	17
36	Nb^{4+}	Nb^{5+}	23
36	Nb^{4+}	Nb^{5+}	23
9	Nb^{4+}	Nb^{5+}	17
20	Nb^{4+}	Nb^{4+}	3
21	Nb^{5+}	Nb^{5+}	17
25	Nb^{5+}	Nb^{5+}	23

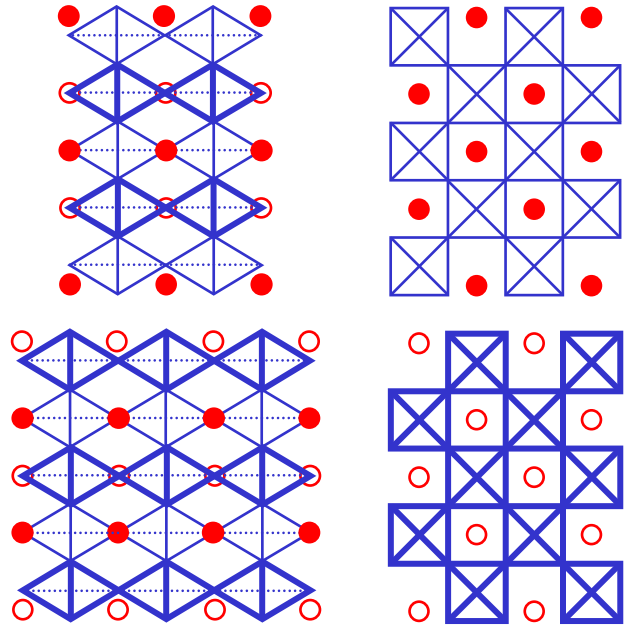

Light and heavy drawing of the BO_6 octahedra and BO_4 polyhedra as well as filled and open circles indicate a height difference perpendicular to the drawing plane

$SrNbO_{3.2} \triangleq Sr_5Nb_5O_{16} \triangleq Sr_{20}Nb_{20}O_{64}$
Non-centrosymmetric ! • Space Group No 31
Probably also a quasi-1D metal

K. Schückel and Hk. Müller-Buschbaum
Z. Anorg. Allg. Chem. 528 (1985) 91

$Nb^{5+} / 4d^0$
$Nb^{4+} / 4d^1$

F. Lichtenberg et al., Progress in Solid State Chem. 36 (2008) 253

$SrNbO_{3.4} \triangleq Sr_5Nb_5O_{17} \triangleq Sr_{20}Nb_{20}O_{68}$
Centrosymmetric • Space group No. 58
Quasi-1D metal

S. C. Abrahams et al.
Acta Cryst. B 54 (1998) 399

The crystal structure of the n = 5 (II) type $Sr_{20}Nb_{20}O_{64}$

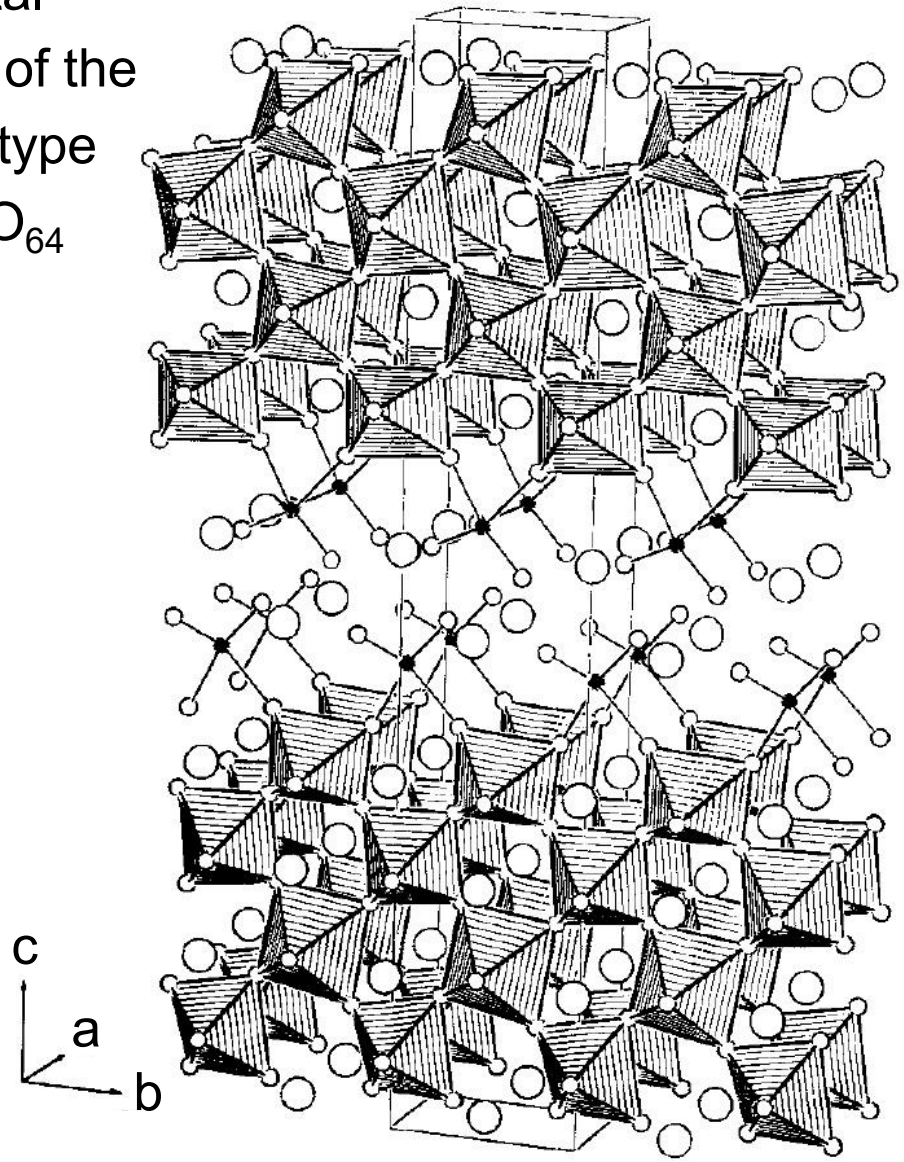

Three-dimensional representation of the non-centrosymmetric crystal structure of $SrNbO_{3.2} \triangleq Sr_5Nb_5O_{16} \triangleq Sr_{20}Nb_{20}O_{64}$ from the paper of K. Schückel and Hk. Müller-Buschbaum [1].

The O ions are depicted as small open balls, the Nb ions as small black balls, and the Sr ions as large open balls. The hatched objects represent the NbO_6 octahedra.

The definition of the specified a-, b-, and c-axis is not the same as in the paper from K. Schückel and Hk. Müller-Buschbaum but in agreement with the used definition on the previous pages.

Image source:

[1] Ein weiteres gemischtvalentes Oxoniobat: $Sr_5Nb_3^{4+}Nb_2^{5+}O_{16}$
K. Schückel and Hk. Müller-Buschbaum
Zeitschrift für anorganische und allgemeine Chemie
528 (1985) 91 – 97
Paper in German but title and abstract also in English
https://doi.org/10.1002/zaac.19855280909

First it was intended to study the melt-grown $Sr_{17}CaBaNb_{19}WO_{64}$ (sample No. 838) by single crystal x-ray diffraction. However, it was not possible to prepare from the melt-grown material small crystals with a suitable size and shape because the material displays a pronounced cleavage behavior. It suggests the presence of a particular weak bond strength between the layers that might result from the Sr- and O vacancies which are most probably located at the boundary of the layers.

Then it was tried to study the melt-grown $Sr_{17}CaBaNb_{19}WO_{64}$ by electron diffraction.

An analysis of melt-grown $Sr_{17}CaBaNb_{19}WO_{64}$ by Scanning Electron Microscopy (SEM), Energy-Dispersive x-ray Spectroscopy (EDS), and Transmission Electron Microscopy (TEM) indicates the presence of a single phase material. This is in accordance with the results from an analysis by powder x-ray diffraction [5].

The similarity of the non-centrosymmetric structure (space group $Pmn2_1$ / No. 31) and centrosymmetric structure (space group Pnnm / No. 58) makes a symmetry analysis difficult.

The simulation of the powder x-ray diffraction pattern of the parent compounds $Sr_{20}Nb_{20}O_{68}$ (centrosymmetric, space group Pnnm / No. 58) and $Sr_{20}Nb_{20}O_{64}$ (non-centrosymmetric, space group $Pmn2_1$ / No. 31) indicates the presence of peaks in the non-centrosymmetric phase which do not appear in the centrosymmetric phase. Based on those reflections a lamella was prepared with an [100] orientation by using the Focused Ion Beam (FIB) technique. That allows the detection of those specific peaks in the low symmetry phase by comparing the results of simulated and experimental of the electron diffraction patterns of the respective structures acquired by TEM.

Both experimental and simulated diffraction results show that the (050) peak, a characteristic Bragg peak of the non-centrosymmetric structure, which is absent in the centrosymmetric structure, can be observed in the experimental electron diffraction pattern. It indicates that the melt-grown material $Sr_{17}CaBaNb_{19}WO_{64}$ displays a non-centrosymmetric structure. The magnetic susceptibility $\chi(T)$ of $Sr_{17}CaBaNb_{19}WO_{64}$ suggests it is a quasi-1D metal [5] and because of its non-centrosymmetric structure it is most probably a polar or ferroelectric quasi-1D metal.

Note: On this page and in part 3 the above-mentioned (050) peak refers to a definition where the b-axis is the longest axis, whereas on pages 5, 6, and 10 – 15 and in Refs. [2, 4 – 8] the *c*-axis is defined as the longest axis

2 Experimental ...

Experimental

From a piece of the melt-grown material some lamellae for TEM investigations were prepared by the Focused Ion Beam (FIB) technique using a dual beam Gallium FIB-SEM of the type FEI Helios 600i. The Energy-dispersive X-ray Spectroscopy (EDS) was performed in another SEM.

Transmission Electron Microscopy (TEM) and Scanning Transmission Electron Microscopy (STEM) experiments were performed with a JEOL F200 STEM / TEM at 200 kV. Simulation of TEM images were performed with the JEMS simulation package, and STEM images with the Dr. Probe software.

JEMS: https://www.jems-swiss.ch/default.htm
Dr. Probe: https://er-c.org/barthel/drprobe

3 Results ...

Study of melt-grown $Sr_{17}CaBaNb_{19}WO_{64}$ (sample No. 838) with respect to the structure of $Sr_5Nb_5O_{17} \triangleq Sr_{20}Nb_{20}O_{68}$ and $Sr_5Nb_5O_{16} \triangleq Sr_{20}Nb_{20}O_{64}$

$Sr_5Nb_5O_{17}$	$Sr_5Nb_5O_{16}$
ICSD database code 54058	ICSD database code 48207
Centrosymmetric	Non- centrosymmetric
a = 32.4560(50) Å	a = 3.992(1) Å
b = 5.674(2) Å	b = 32.476(10) Å
c 3.995(2) Å	c = 5.677(2) Å
α = 90 °	α = 90 °
β = 90 °	β = 90 °
γ = 90 °	γ = 90 °
V = 735.7 Å^3	V = 735.99 Å^3
Number of unit cells per formula unit: Z = 2	Number of unit cells per formula unit: Z = 2
Space group P n n m (No. 58)	Space group P m n 2_1 (No. 31)

Note: The definition of the *a*- , *b*- , and *c*-axis in the left and right column is different. It is the same which is used in Ref. [3] and [1], respectively. On pages 5, 6 and 10 – 15 and in Refs. [2, 4 – 8] the *c*-axis is defined as the longest axis

SEM image and the area for an Electron Back Scatter Diffraction (EBSD) analysis

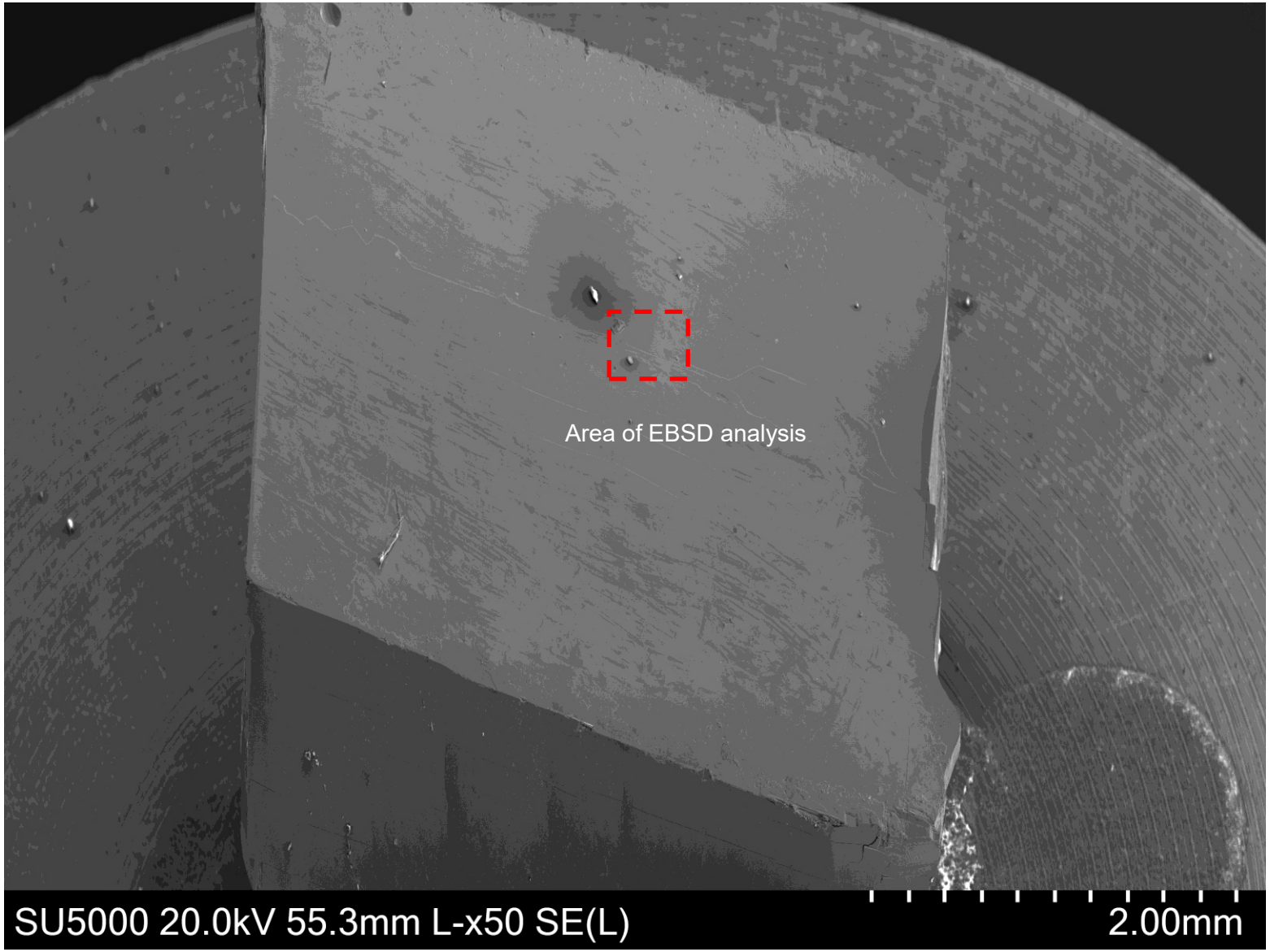

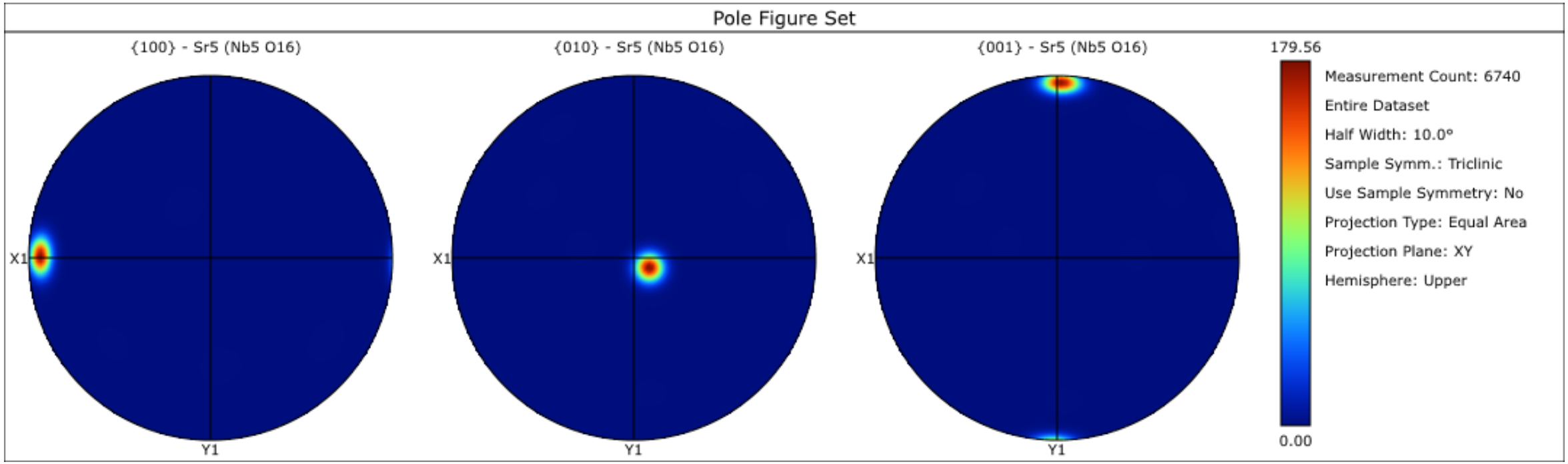

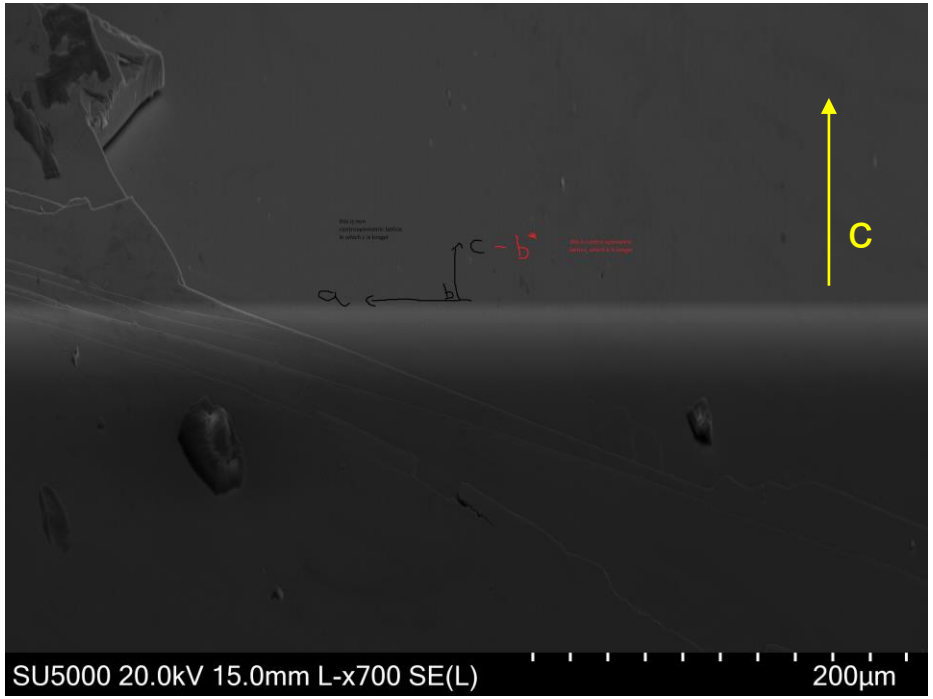

Left: SEM image with enhanced resolution when compared to that on the previous page

Top: From pole figure analysis with space group No. 31 the normal to the surface of the melt-grown material is along the b-axis. In this case the b-axis is defined as the longest axis.

Two ways to prepare a FIB lamella with a direction of [001] or [100]

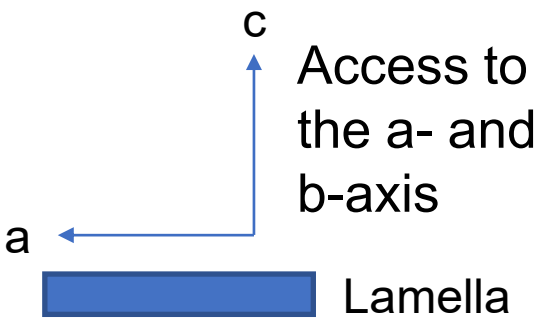

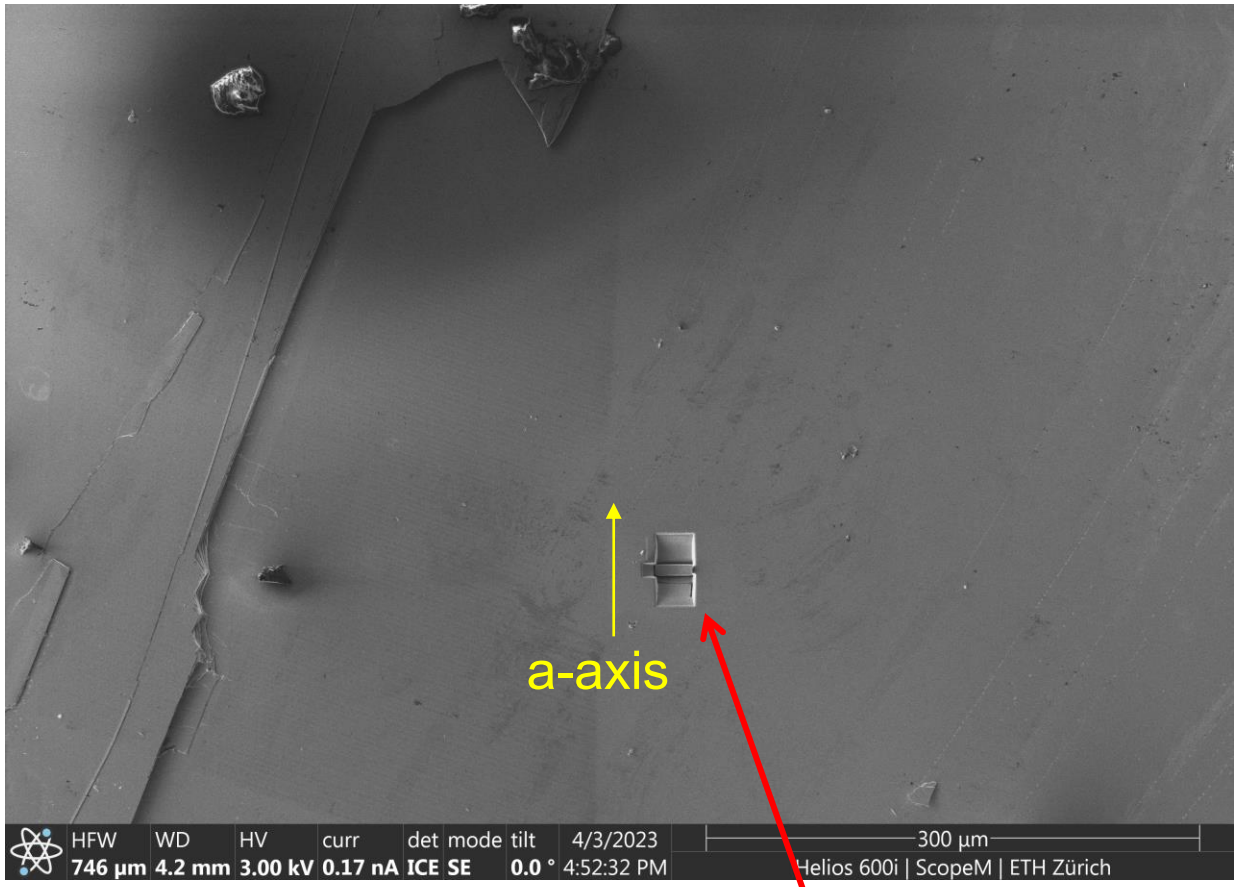

SEM image and the FIB lamella position in the sample

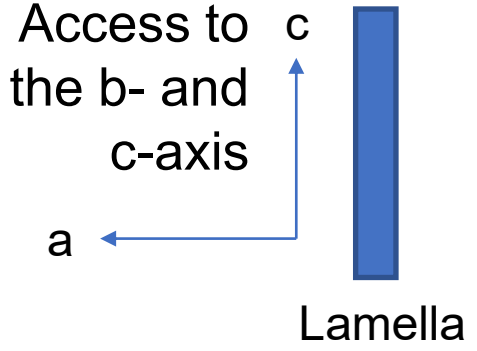

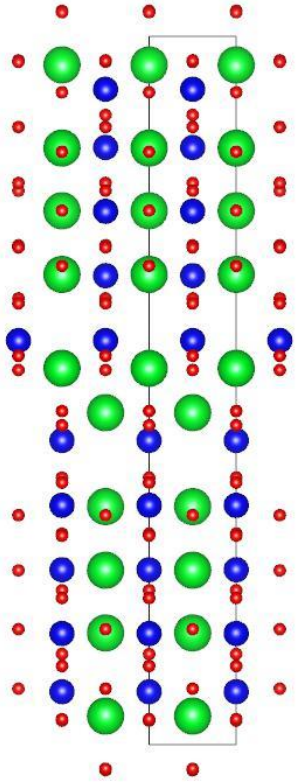

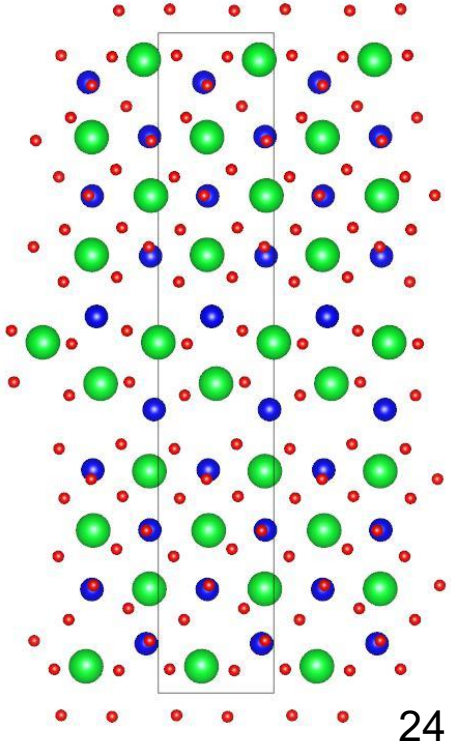

TEM images of the lamella after FIB preparation

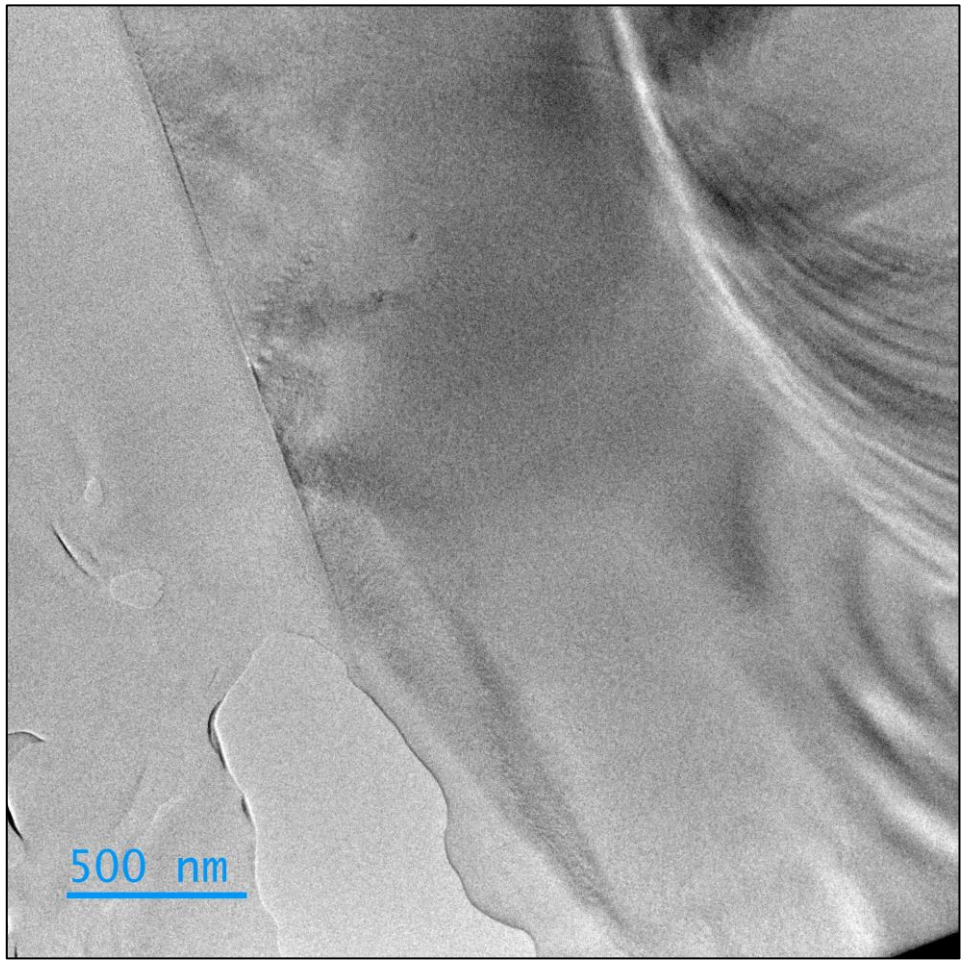

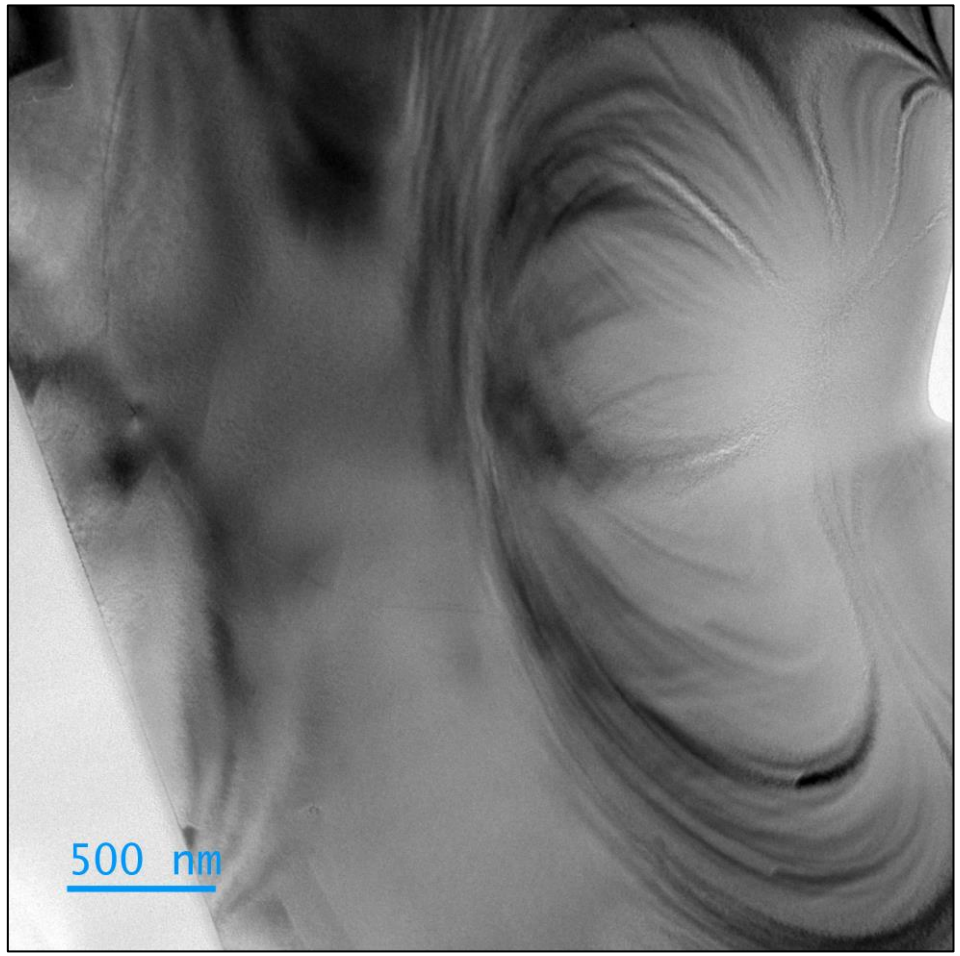

The left image is a normal bright field image and the right one is the lower magnification bright field image with an introduced contrast aperture to enhance the contrast of the image for better visibility of potential defects or lattice distortions in the structure of the crystal

High-resolution TEM images of the sample display a nearly uniform lattice and only a few dislocations

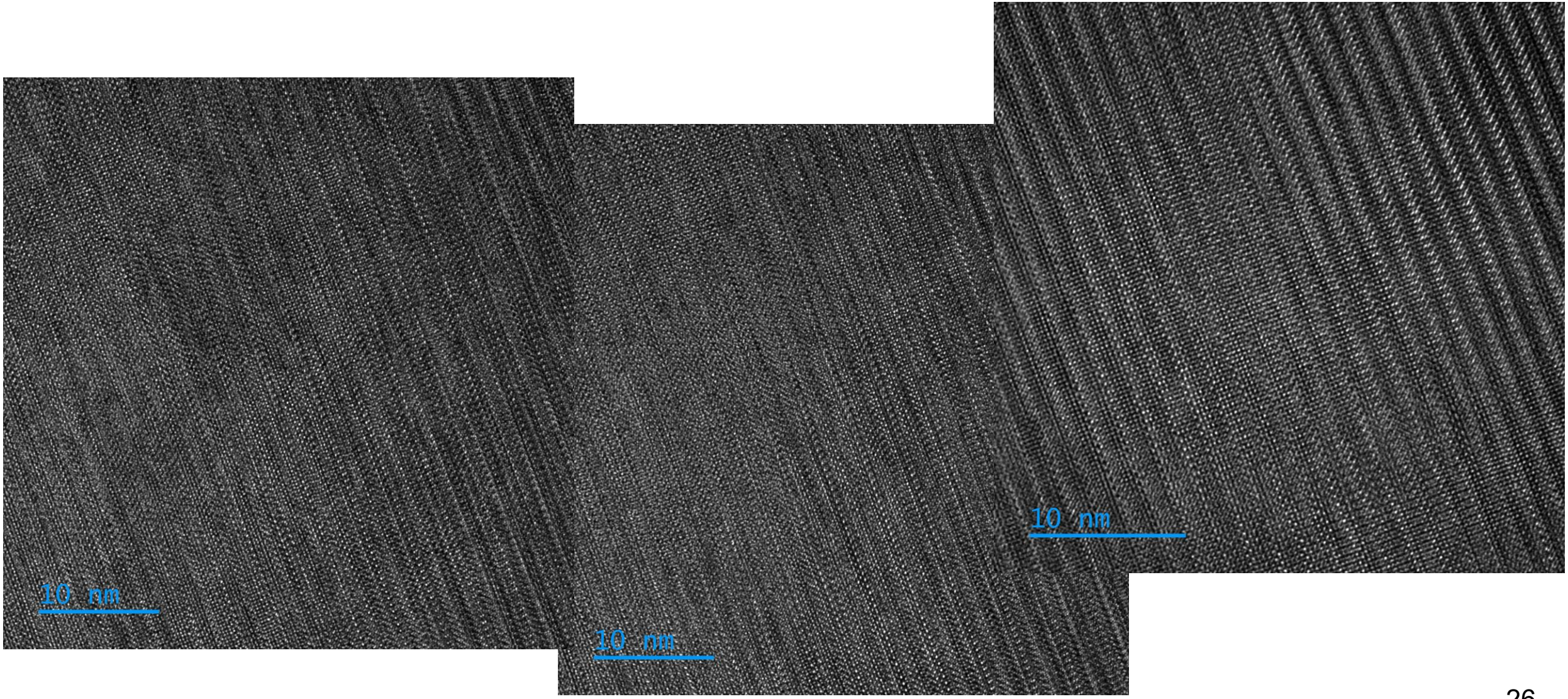

What is the difference between the centrosymmetric and non-centrosymmetric unit cell ?

The Wyckoff positions of the two unit cells from the ICSD crystallography database

Space group P n n m (No. 58)

Nb1	Nb4+	2	a	0.5	0.5	0.5	0.0038(1)	1
Nb2	Nb4+	4	g	0.32264(1)	0.53323(8)	0.5	0.0054(1)	1
Nb3	Nb4+	4	g	0.40931(1)	0.00527(7)	0.5	0.0040(1)	1
Sr1	Sr2+	4	g	0.21466(2)	0.5632(1)	0.5	0.0152(1)	1
Sr2	Sr2+	2	d	0.5	0	0	0.0085(1)	1
Sr3	Sr2+	4	g	0.41129(2)	0.4996(1)	0	0.0083(1)	1
O1	O2-	4	g	0.5374(1)	0.2269(7)	0.5	0.0133(7)	1
O2	O2-	4	g	0.4522(1)	0.2691(6)	0.5	0.0088(6)	1
O3	O2-	2	b	0.5	0.5	0	0.0149(11)	1
O4	O2-	4	g	0.2091(2)	0.2975(7)	0	0.0141(8)	1
O5	O2-	4	g	0.1208(1)	0.2077(7)	0	0.0085(6)	1
O6	O2-	4	g	0.1328(2)	0.7233(8)	0	0.0195(10)	1
O7	O2-	4	g	0.2799(1)	0.3159(7)	0.5	0.0102(6)	1
O8	O2-	4	g	0.3308(1)	0.5047(11)	0	0.0177(9)	1
O9	O2-	4	g	0.4165(1)	-.0104(9)	0	0.0146(8)	1

Centrosymmetric unit cell

Space group P m n 2_1 (No. 31)

Nb1	Nb4+	2	a	0	0.0747(3)	0.1055(25)	0.42(14)	1
Nb2	Nb4+	2	a	0	0.1569(3)	0.5759(24)	0.15(14)	1
Nb3	Nb4+	2	a	0	0.2470(4)	0.0731(32)	0.38(10)	1
Nb4	Nb5+	2	a	0	0.3379(3)	0.5674(27)	0.78(18)	1
Nb5	Nb5+	2	a	0	0.4295(3)	0.0367(25)	0.66(17)	1
Sr1	Sr2+	2	a	0.5	0.0404(3)	0.6263(17)	1.22(17)	1
Sr2	Sr2+	2	a	0.5	0.1578(3)	0.0783(28)	1.21(19)	1
Sr3	Sr2+	2	a	0.5	0.2463(4)	0.5639(29)	0.76(13)	1
Sr4	Sr2+	2	a	0.5	0.3361(3)	0.0777(24)	0.23(14)	1
Sr5	Sr2+	2	a	0.5	0.4687(3)	0.5	0.57(13)	1
O1	O2-	2	a	0	0.128(2)	0.259(9)	0.2(6)	1
O2	O2-	2	a	0	0.034(2)	0.342(8)	1.5(7)	1
O3	O2-	2	a	0	0.111(2)	0.777(8)	1.4(7)	1
O4	O2-	2	a	0	0.207(2)	0.867(8)	1.9(8)	1
O5	O2-	2	a	0	0.218(2)	0.362(8)	0.2(6)	1
O6	O2-	2	a	0	0.036(2)	0.901(8)	0.6(6)	1
O7	O2-	2	a	0	0.471(2)	0.251(9)	1.0(7)	1
O8	O2-	2	a	0	0.295(2)	0.815(9)	1.3(7)	1
O9	O2-	2	a	0	0.377(2)	0.322(8)	1.5(7)	1
O10	O2-	2	a	0	0.451(2)	0.772(8)	1.8(8)	1
O11	O2-	2	a	0	0.298(2)	0.310(9)	0.3(6)	1
O12	O2-	2	a	0	0.370(2)	0.860(9)	1.4(8)	1
O13	O2-	2	a	0.5	0.246(2)	0.104(8)	1.2(7)	1
O14	O2-	2	a	0.5	0.163(2)	0.562(9)	0.0(5)	1
O15	O2-	2	a	0.5	0.324(1)	0.582(9)	0.5(6)	1
O16	O2-	2	a	0.5	0.079(1)	0.076(9)	0.5(6)	1

Non-centrosymmetric unit cell

The general Wyckoff positions of the two unit cells calculated from space group *

Space group P n n m (No. 58)

Multiplicity	Wyckoff letter	Site symmetry	Coordinates
8	h	1	(x,y,z) (-x,-y,z) (-x+1/2,y+1/2,-z+1/2) (x+1/2,-y+1/2,-z+1/2) (-x,-y,-z) (x,y,-z) (x+1/2,-y+1/2,z+1/2) (-x+1/2,y+1/2,z+1/2)
4	g	..m	(x,y,0) (-x,-y,0) (-x+1/2,y+1/2,1/2) (x+1/2,-y+1/2,1/2)
4	f	..2	(0,1/2,z) (1/2,0,-z+1/2) (0,1/2,-z) (1/2,0,z+1/2)
4	e	..2	(0,0,z) (1/2,1/2,-z+1/2) (0,0,-z) (1/2,1/2,z+1/2)
2	d	..2/m	(0,1/2,1/2) (1/2,0,0)
2	c	..2/m	(0,1/2,0) (1/2,0,1/2)
2	b	..2/m	(0,0,1/2) (1/2,1/2,0)
2	a	..2/m	(0,0,0) (1/2,1/2,1/2)

Space group P m n 2_1 (No. 31)

Multiplicity	Wyckoff letter	Site symmetry	Coordinates
4	b	1	(x,y,z) (-x+1/2,-y,z+1/2) (x+1/2,-y,z+1/2) (-x,y,z)
2	a	m..	(0,y,z) (1/2,-y,z+1/2)

Red colors show the Wyckoff positions which are not in our unit cell.

* Calculated from https://www.cryst.ehu.es/cgi-bin/cryst/programs/symm_modes

Wyckoff positions continued ...

Wyckoff positions of group *Pnnm*(58)

Only bold Wyckoff positions are considered according to unit cell

WP	Representatives
8h	x,y,z
4g	**x,y,0**
4f	0,1/2,z
4e	0,0,z
2d	**0,1/2,1/2**
2c	0,1/2,0
2b	**0,0,1/2**
2a	**0,0,0**

Wyckoff Positions Splitting for group - subgroup pair *Pnnm*(58)>*Pmn*2_1(31)

The group subgroup chain you want to consider is characterized by:

- an index 2;
- a transformation matrix which relates the coordinate system of the subgroup to that of the supergroup:

$$\begin{bmatrix} 0 & 0 & 1 \\ 0 & 1 & 0 \\ -1 & 0 & 0 \end{bmatrix} \begin{bmatrix} 0 \\ 1/4 \\ 0 \end{bmatrix}$$

Result from splitting

No	Wyckoff position(s)	
	Group	Subgroup
1	4g	2a 2a
2	2d	2a
3	2b	2a
4	2a	2a

→ From a symmetry analysis of the parent-child groups it is difficult to draw a conclusion on which specific Wyckoff position we should look at because the low symmetry structure (space group No. 31) has only the Wyckoff position 2a for all elements

Simulation of the powder x-ray diffraction pattern by VESTA Version 3.5.8 *

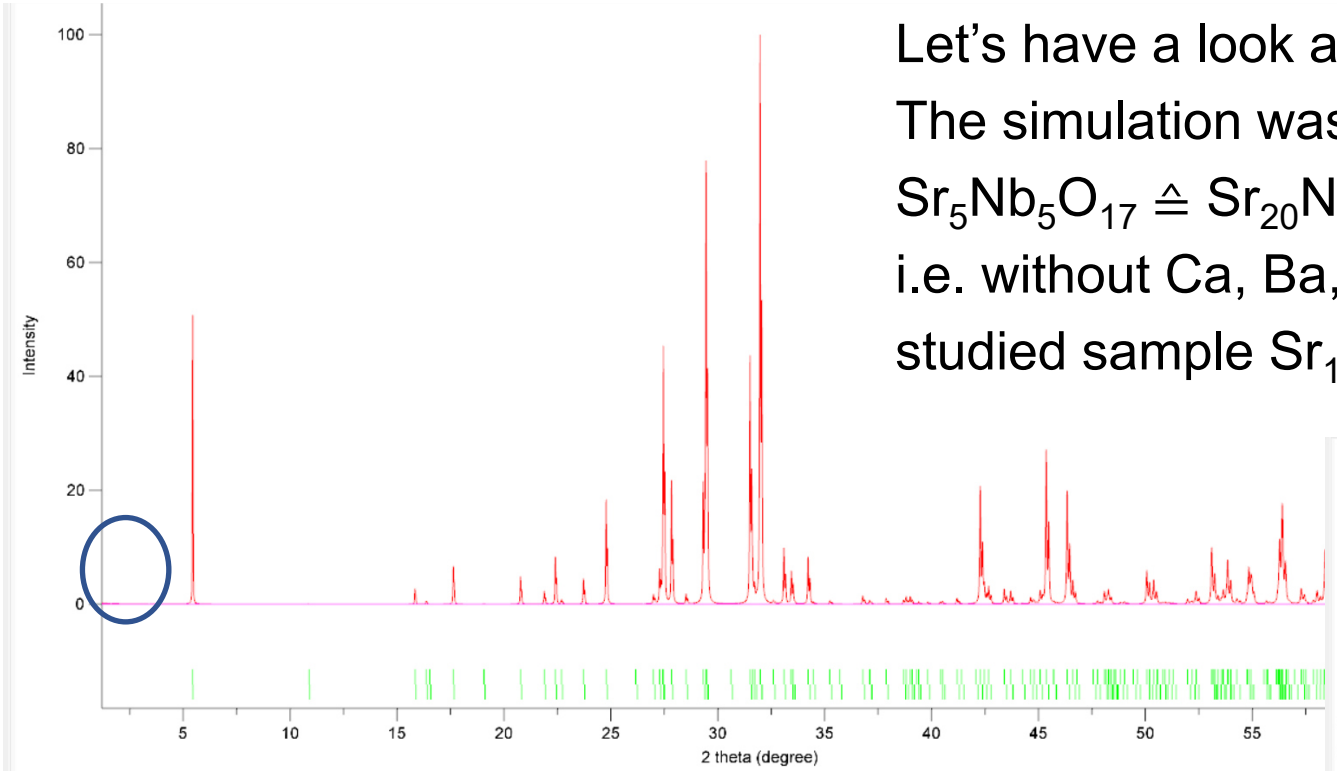

Let's have a look at missing reflections in the two unit cells.
The simulation was done with respect to
$Sr_5Nb_5O_{17} \triangleq Sr_{20}Nb_{20}O_{68}$ and $Sr_5Nb_5O_{16} \triangleq Sr_{20}Nb_{20}O_{64}$,
i.e. without Ca, Ba, W, and the Sr-deficiencies in the studied sample $Sr_{17}CaBaNb_{19}WO_{64}$

ICSD database code 54058: $Sr_5Nb_5O_{17}$

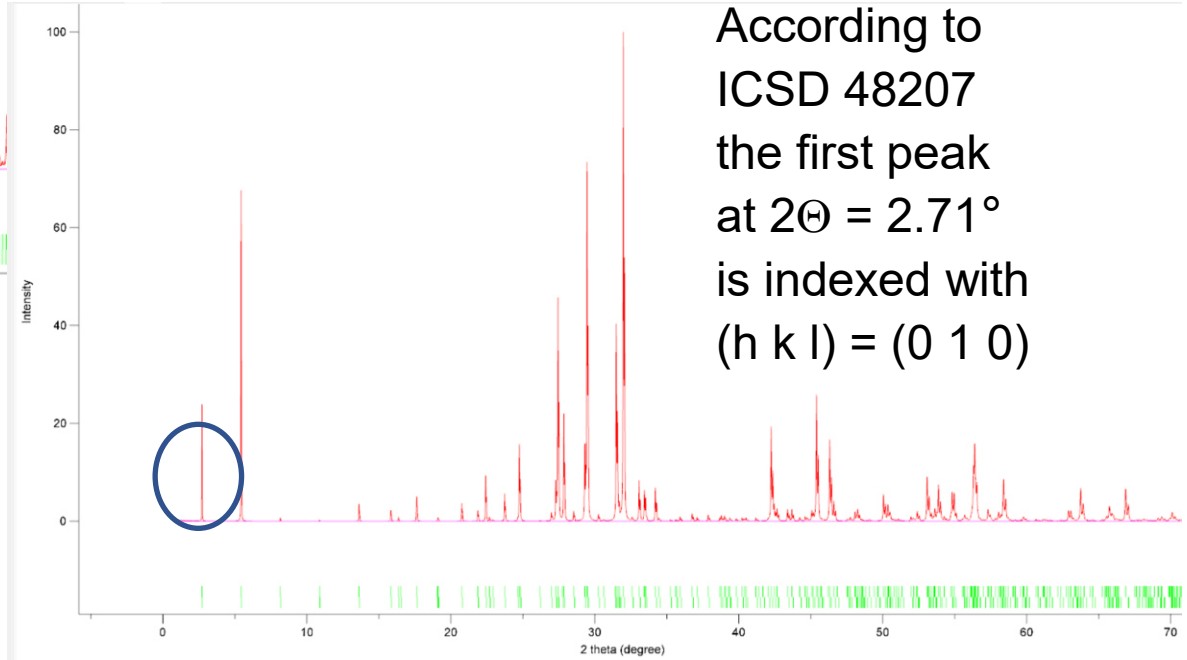

According to ICSD 48207 the first peak at $2\Theta = 2.71°$ is indexed with (h k l) = (0 1 0)

ICSD database code 48207: $Sr_5Nb_5O_{16}$

* VESTA: https://jp-minerals.org/vesta/en

Simulation of the powder x-ray diffraction pattern by VESTA Version 3.5.8 *

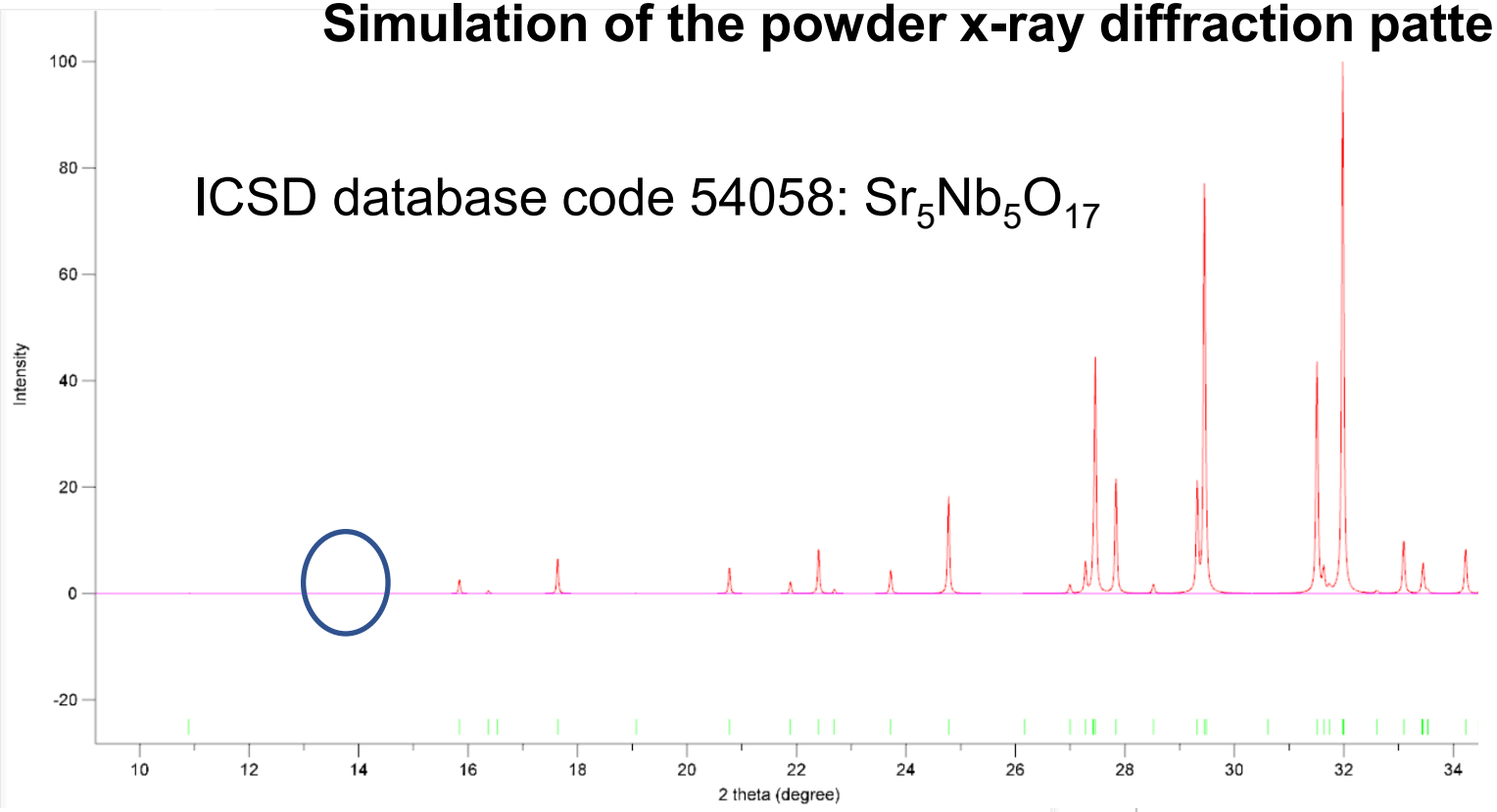

According to
ICSD 48207
the second peak
at 2Θ = 13.62°
is indexed with
(h k l) = (0 5 0)

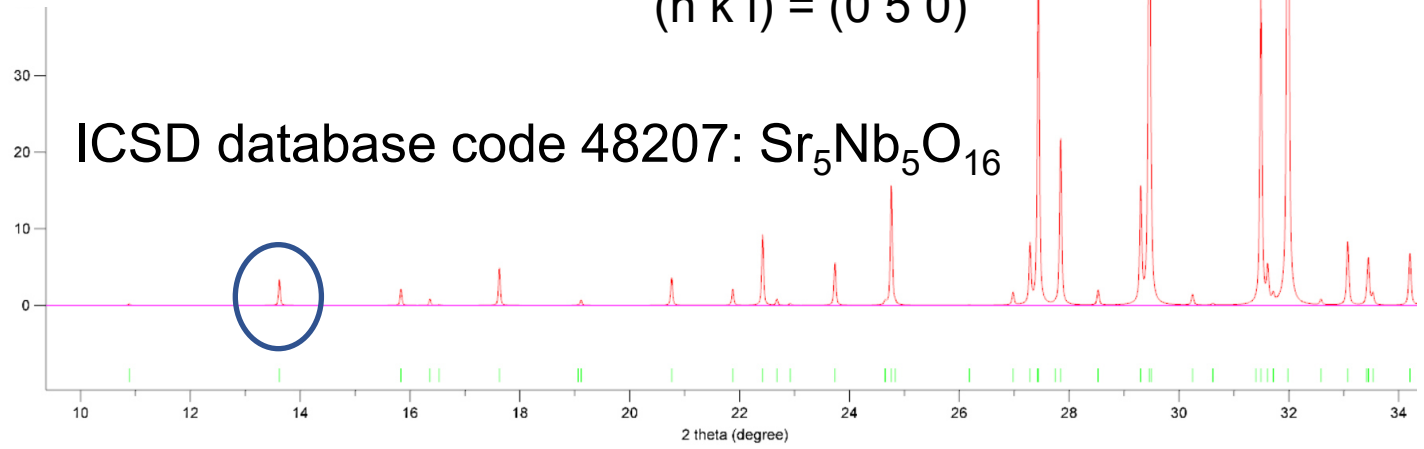

* VESTA: https://jp-minerals.org/vesta/en

Simulation of the powder x-ray diffraction pattern by VESTA Version 3.5.8 *

ICSD database code 54058: $Sr_5Nb_5O_{17}$

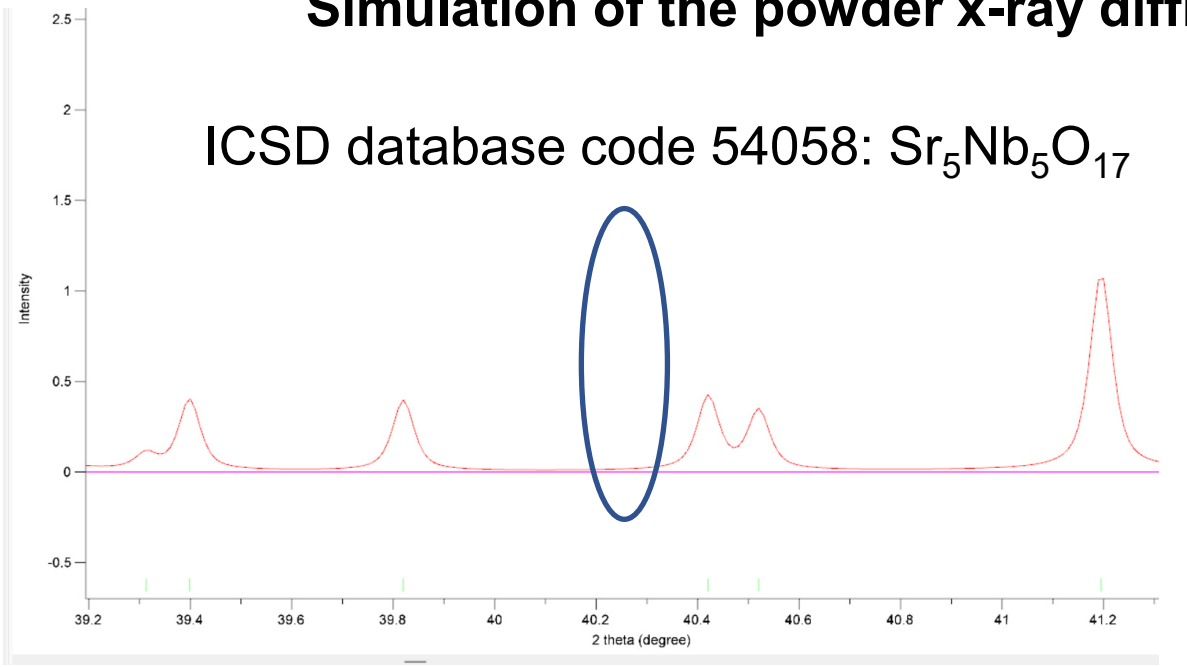

ICSD database code 48207: $Sr_5Nb_5O_{16}$

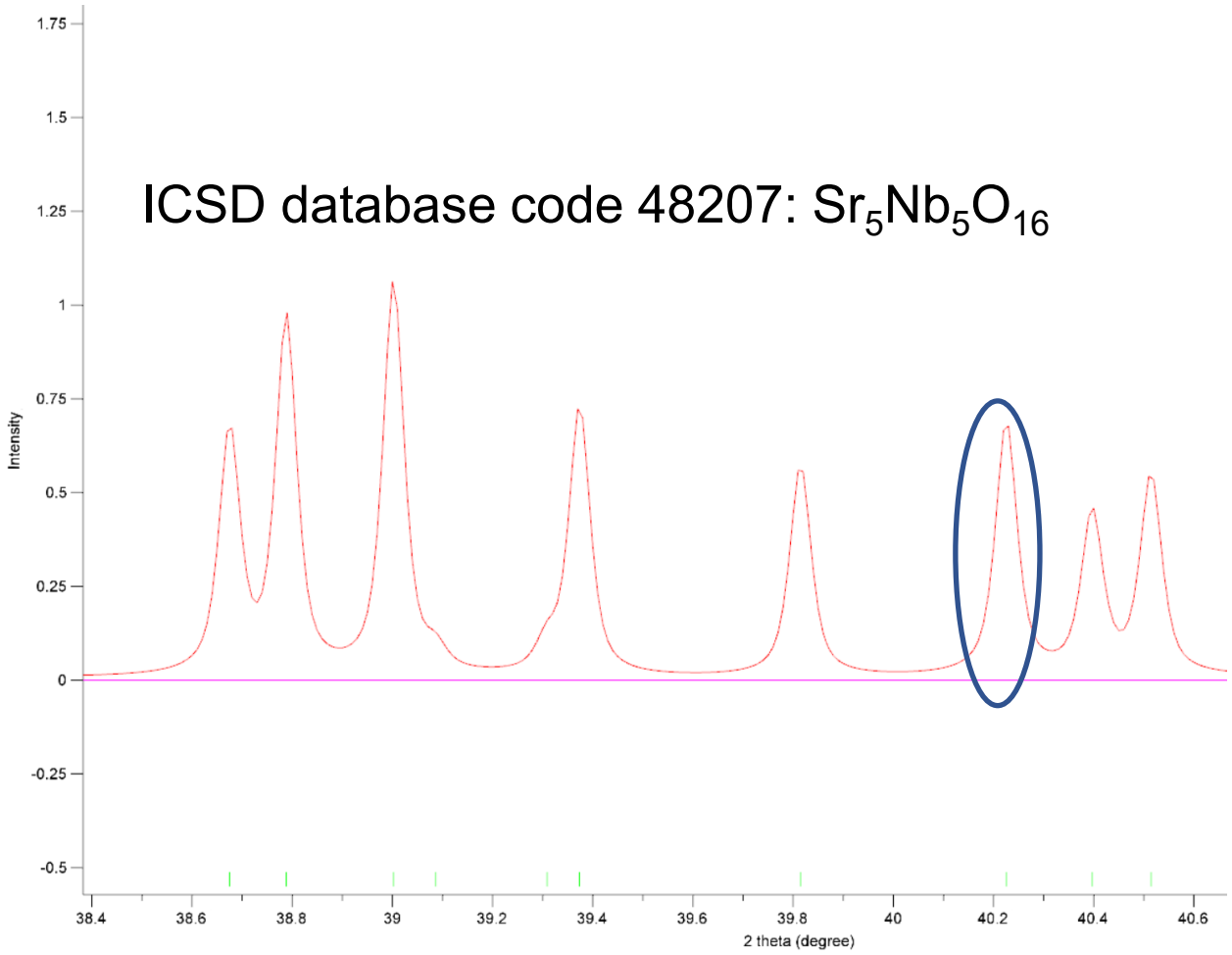

According to
ICSD 48207
the peak at
$2\Theta = 40.22°$
is indexed with
(h k l) = (1 12 0)

* VESTA: https://jp-minerals.org/vesta/en

Comparison of the electron diffraction patterns and if the missing peaks are observed or not

Simulation of the diffraction pattern by Single Crystal Version 4.1.9 * of the space group No. 58 and 31 along the [001] and [100] zone axis, respectively. Note that the zone axis is the same in both cases when taking into account the different definitions of the a-, b-, and c-axis, see page 21

Space group P n n m (No. 58)

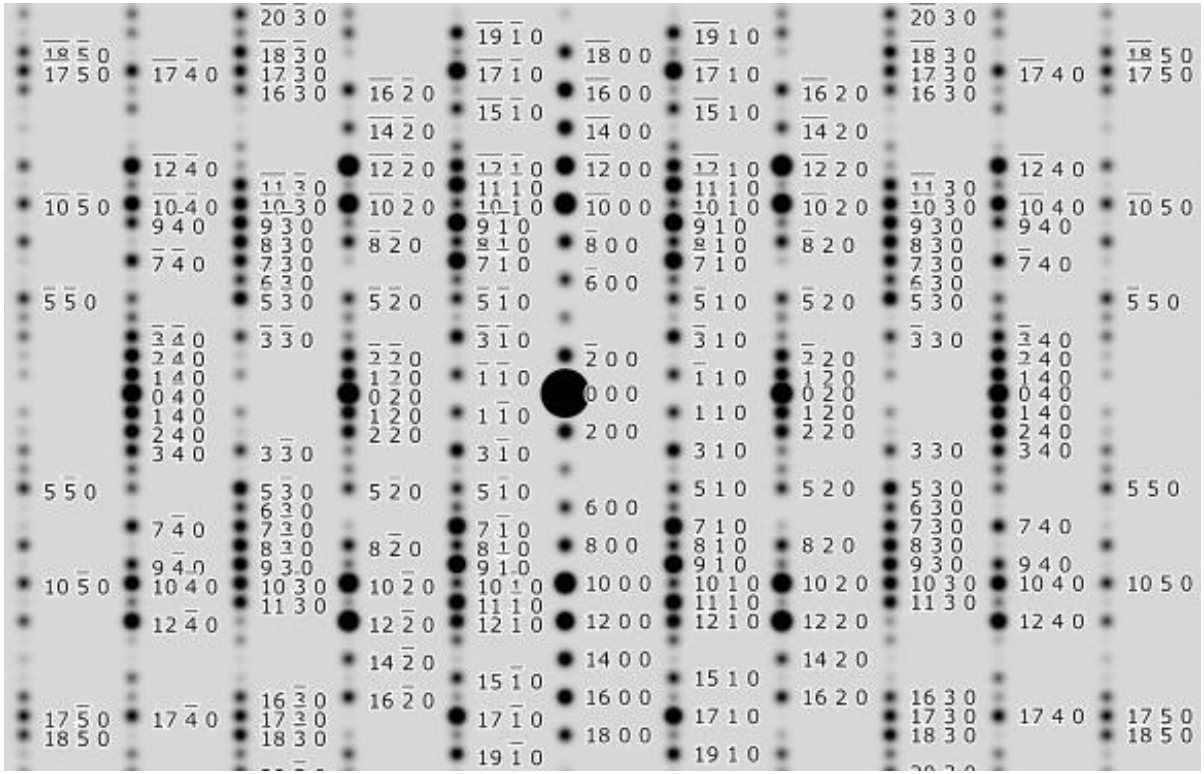

Space group P m n 2_1 (No. 31)

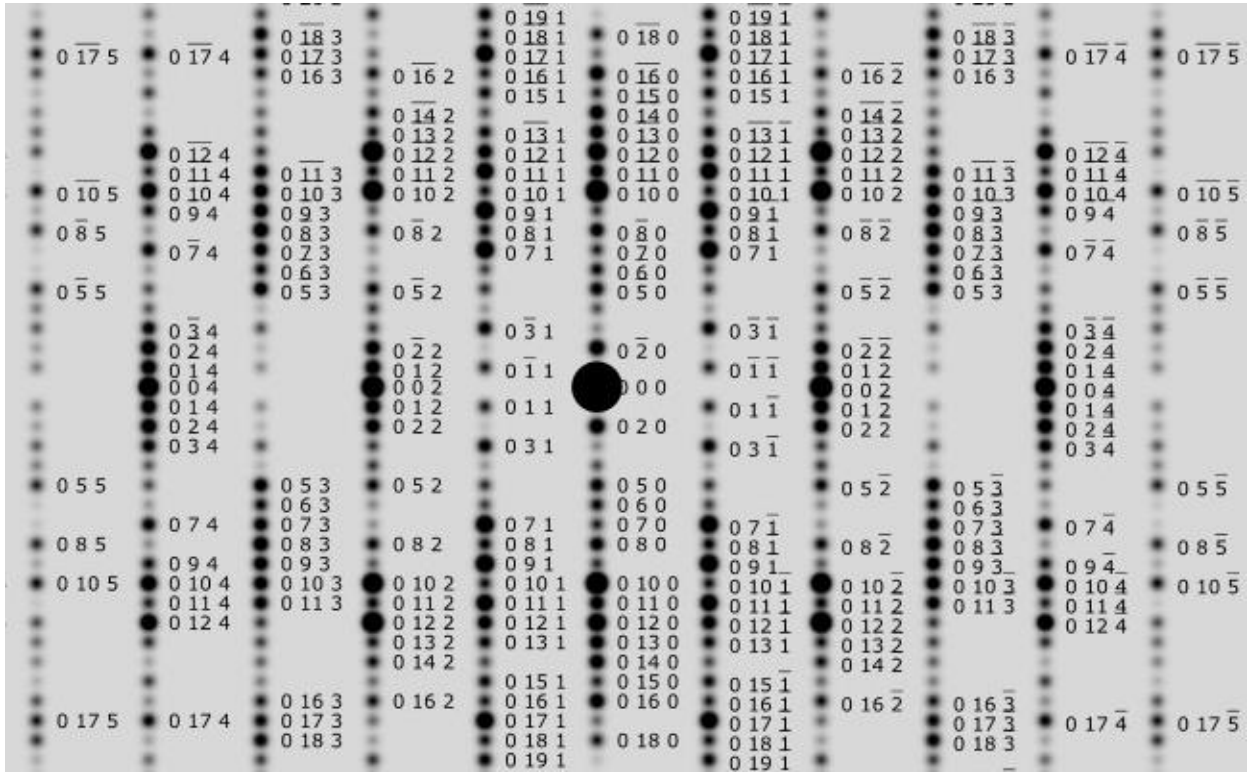

* Single Crystal: https://crystalmaker.com/singlecrystal

Comparison of the electron diffraction patterns and if the missing peaks are observed or not

The same but magnified diffraction patterns to see the details. The (050) reflection is only observed for the non-centrosymmetric space group No. 31 as it was simulated and predicted by the XRD pattern

Space group P n n m (No. 58)

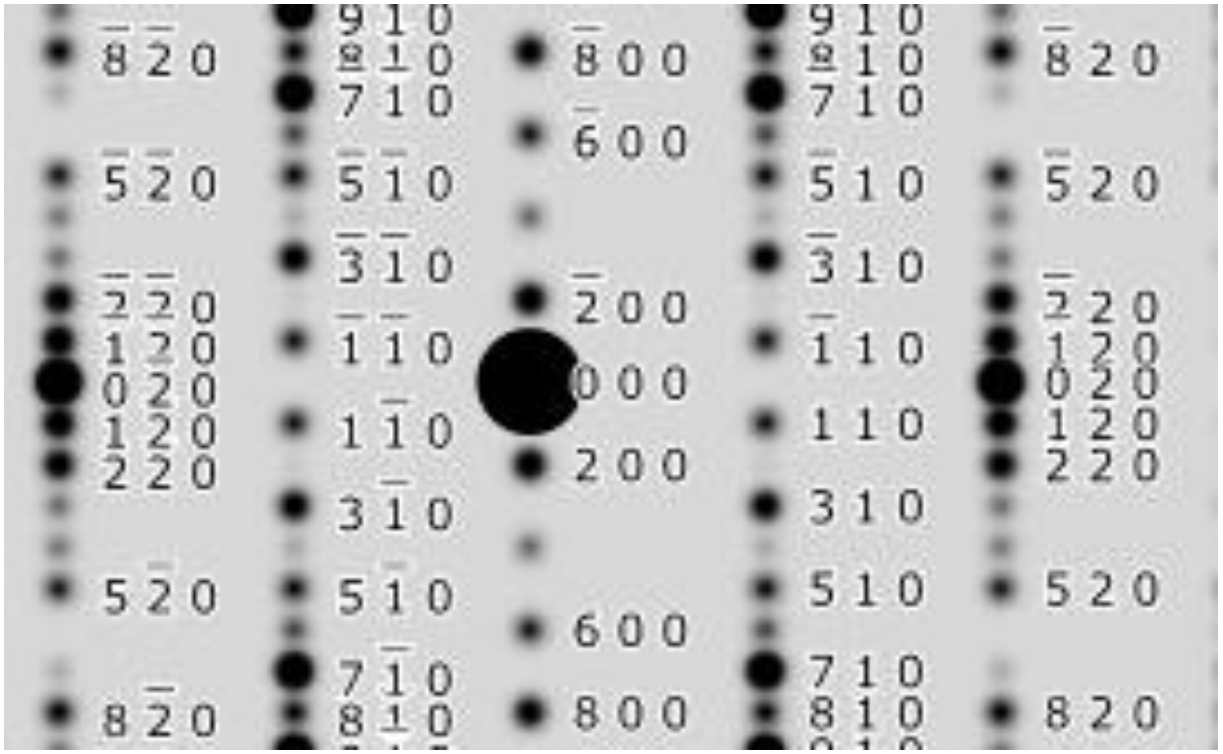

Space group P m n 2_1 (No. 31)

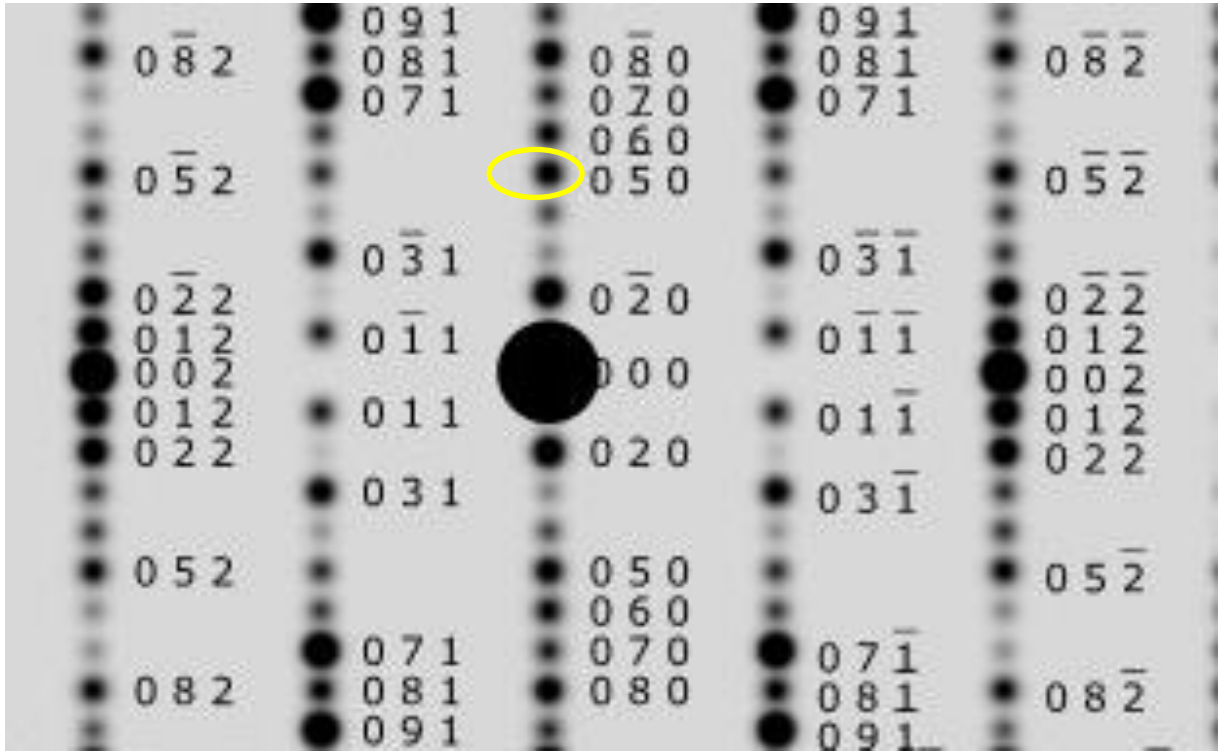

Experimental electron diffraction patterns obtained from two different areas of the lamella

The observations from XRD and electron diffraction pattern simulations match well with the [100] or [001] direction, even if the intensities in the second image are slightly different. Based on EBSD the lamella was prepared with an electron beam parallel to the a-axis, i.e. along the [100] direction

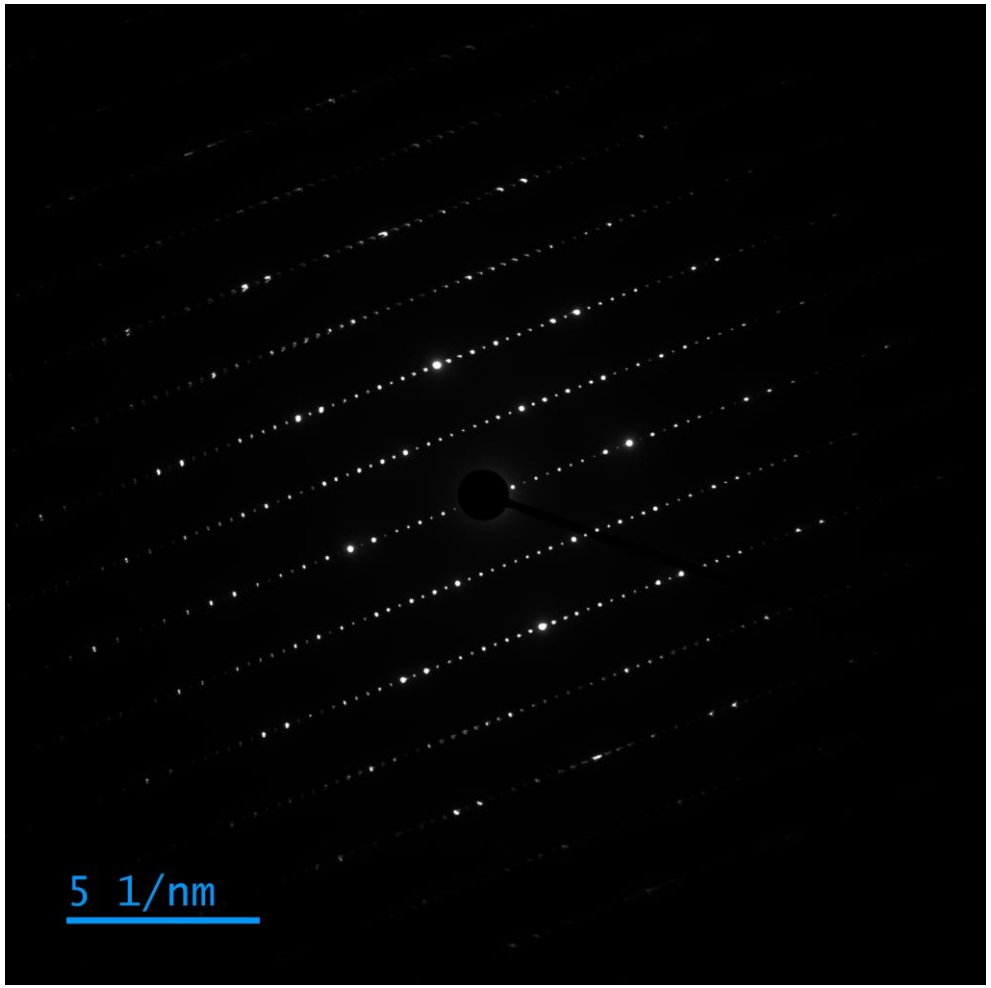

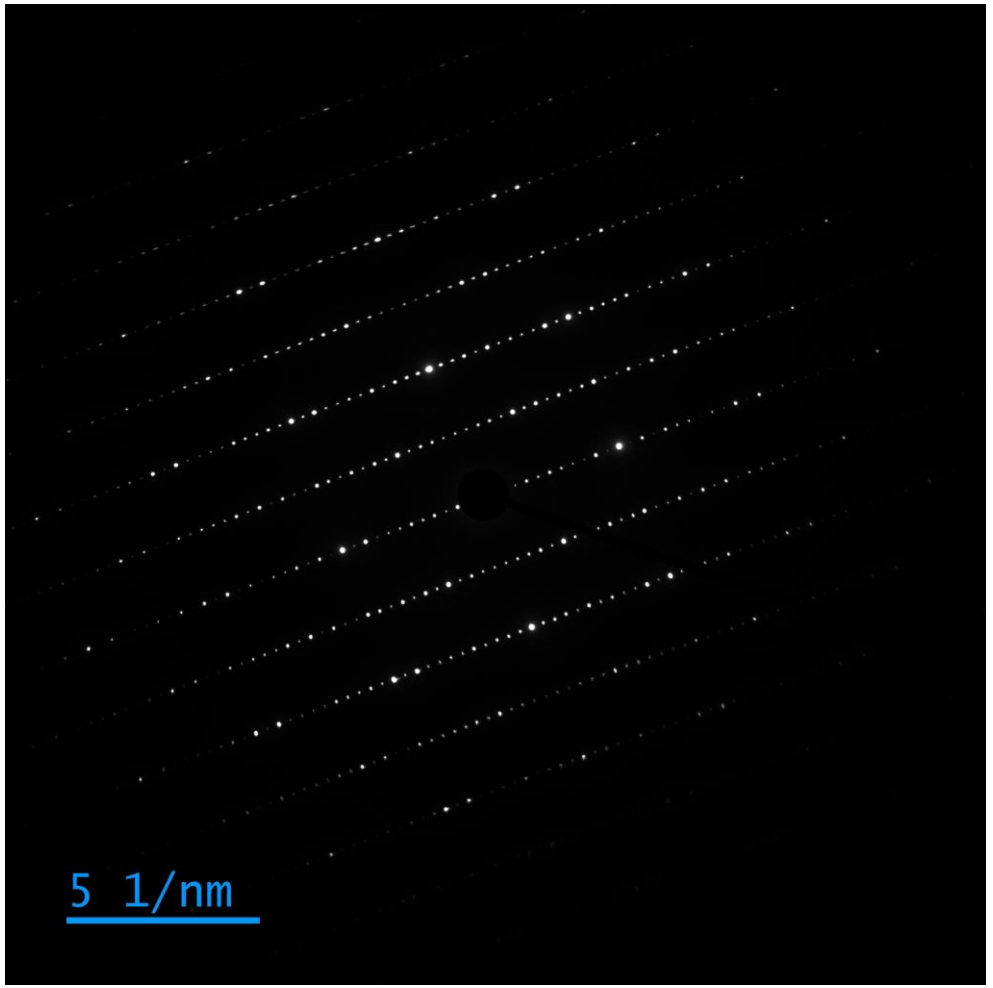

Experimental (left) and simulated (right) electron diffraction pattern

They show the match of the diffraction spots. As expected the intensities in the experimental pattern is slightly different from that in the simulated pattern because of the additional elements Ca, Ba, W and the Sr-deficiencies in the lattice and the slight tilt of the sample.

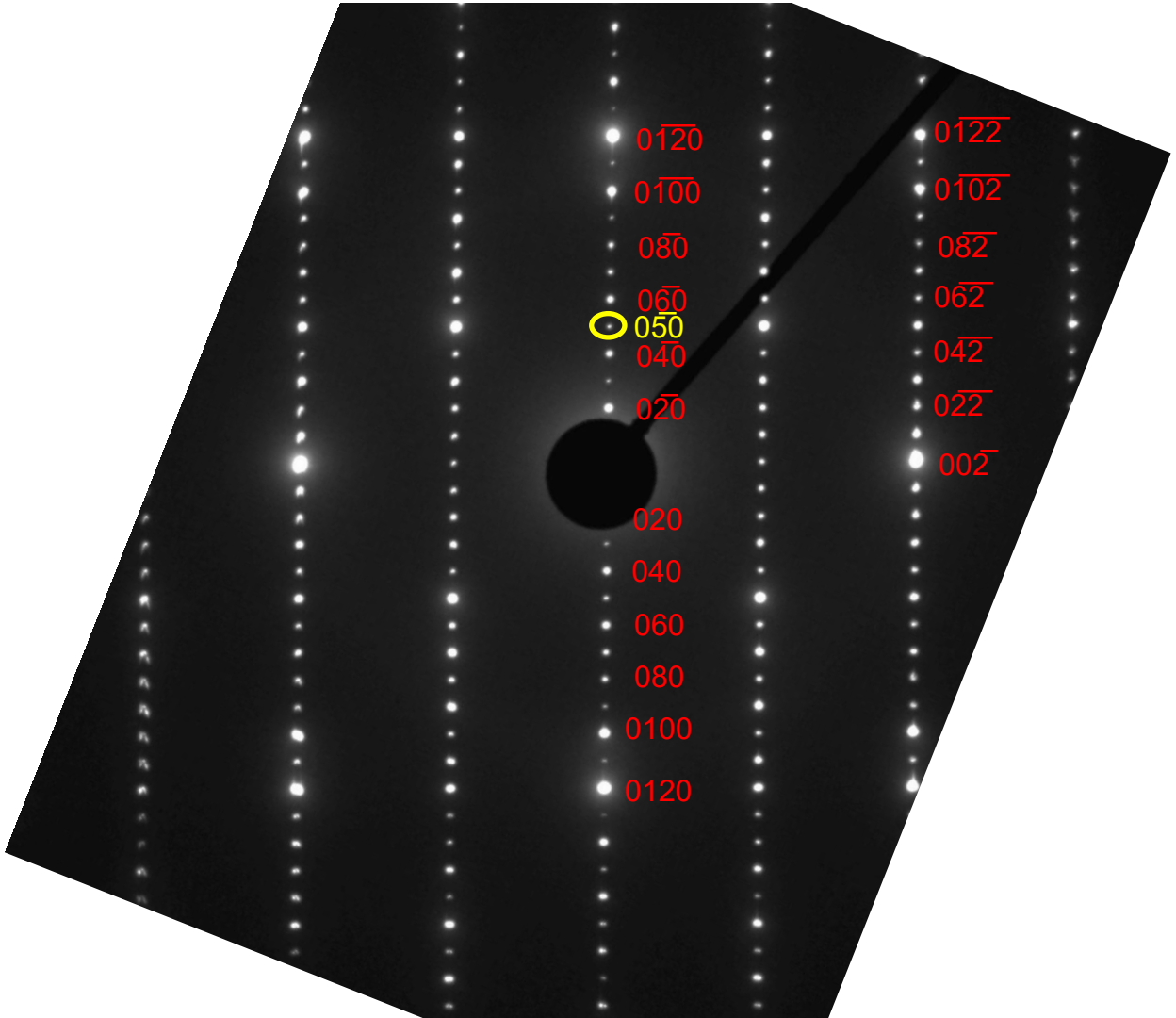

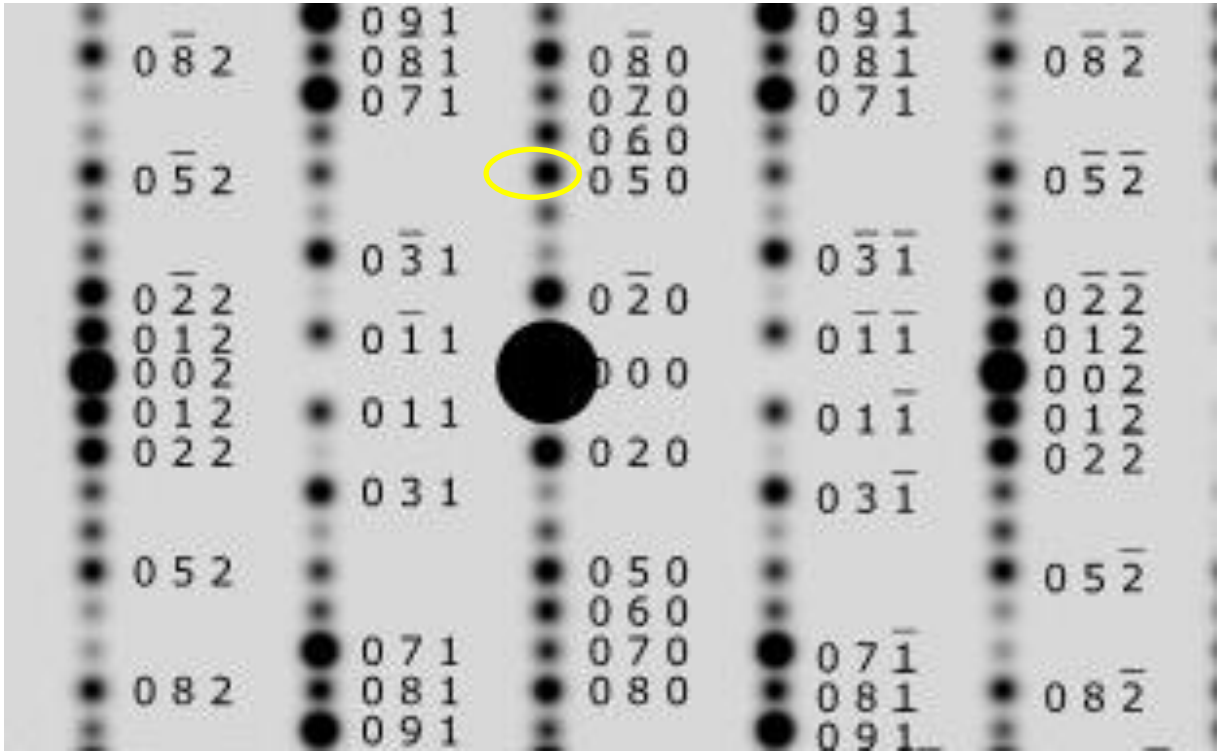

Space group P m n 2_1 (No. 31)

4 Author contributions ...

Author contributions

Ali Baghi Zadeh performed the SEM and TEM experiments and simulations and prepared a report about the results of the crystallographic studies.

Frank Lichtenberg provided pieces of the melt-grown material and its powder x-ray diffraction data and prepared this paper in form of a presentation by using Ali Baghi Zadeh‘s report and parts of Ref. [5].

Christian Zaubitzer prepared from the melt-grown material some lamellae by the FIB technique.

Luiz Grafulha Morales performed the EBSD experiments and analysis.

Arkadiy Simonov tried to prepare from the melt-grown material small crystals which are suitable for single crystal x-ray diffraction.

5 Acknowledgement ...

Acknowledgement

Nicola Spaldin and Frank Lichtenberg thank the ETH Zurich for financial support.

Frank Lichtenberg thanks Nicola Spaldin for her support, Marc Petitmermet for his IT support, and Susanne Blatter for her administrative support.

Ali Baghi Zadeh acknowledges the access to computational resources and software for image analysis at ScopeM.

6 References ...

References 1 / 4

[1] Ein weiteres gemischtvalentes Oxoniobat: $Sr_5Nb_3^{4+}Nb_2^{5+}O_{16}$

K. Schückel and Hk. Müller-Buschbaum

Zeitschrift für anorganische und allgemeine Chemie 528 (1985) 91 - 97

https://doi.org/10.1002/zaac.19855280909

Paper in German but title and abstract also in English

[2] Synthesis, structural, magnetic and transport properties of perovskite-related layered titanates, niobates and tantalates of the type $A_nB_nO_{3n+2}$, $A'A_{k-1}B_kO_{3k+1}$ and $A_mB_{m-1}O_{3m}$

F. Lichtenberg, A. Herrnberger, and K. Wiedenmann

Progress in Solid State Chemistry 36 (2008) 253 – 387

https://dx.doi.org/10.1016/j.progsolidstchem.2008.10.001

[3] Centrosymmetric or non-centrosymmetric ? Case study, Generalization, and Structural Redetermination of $Sr_5Nb_5O_{17}$

S.C. Abrahams, H.W. Schmalle, T. Williams, A. Reller, F. Lichtenberg, D. Widmer, J.G. Bednorz, R. Spreiter, Ch. Bosshard, and P. Gunter

Acta Crystallographica Section B 54 (1998) 399 – 416

https://doi.org/10.1107/S0108768197019642

References 2 / 4

[4] Synthesis of perovskite-related layered $A_nB_nO_{3n+2}$ = ABO_X type niobates and titanates and study of their structural, electric and magnetic properties

F. Lichtenberg, A. Herrnberger, K. Wiedenmann, J. Mannhart

Progress in Solid State Chemistry 29 (2001) 1 – 70

https://dx.doi.org/10.1016/S0079-6786%2801%2900002-4

[5] Carpy-Galy phases $A_nB_nO_{3n+2}$ = ABO_x: Overview, properties, special and hypothetical systems, and melt-grown synthesis of *A*- and O-deficient *n* = 5 types such as $Sr_{19}Nb_{19}WO_{66}$ and $Sr_{17}Ca_2Nb_{19}WO_{64}$ and *n* = 6 type $Ln_6Ti_4Fe_2O_{20}$ and $Ca_6Nb_5FeO_{20}$

Frank Lichtenberg

Published by the library of the ETH Zurich / ETH Research Collection in July 2020 (477 slides or pages)

https://doi.org/10.3929/ethz-b-000424221

References 3 / 4

[6] Photoinduced metastable *dd*-exciton-driven metal-insulator transitions in quasi-one-dimensional transition metal oxides

Teguh Citra Asmara, Frank Lichtenberg, Florian Biebl, Tao Zhu, Pranab Kumar Das, Muhammad Avicenna Naradipa, Angga Dito Fauzi, Caozheng Diao, Ping Yang, Philipp Lenzen, Sören Buchenau, Benjamin Grimm-Lebsanft, Dongyang Wan, Paolo E. Trevisanutto, Mark B. H. Breese, T. Venkatesan, Michael Rübhausen, and Andrivo Rusydi

Communications Physics 3 (2020) article number 206 (1 – 9)

https://doi.org/10.1038/s42005-020-00451-w

[7] Excitonic quenching of the oxygen-chain phonon in the photoinduced metal-to-insulator transition of photoexcited $Sr_{0.95}NbO_{3.37}$ studied by ultraviolet-resonance Raman scattering

Sören Buchenau, Florian Biebl, Benjamin Grimm-Lebsanft, Philipp Lenzen, Teguh C. Asmara, Andrivo Rusydi, Frank Lichtenberg, andMichael Rübhausen

Physical Review B 107 (2023) 035149 (1 – 5)

https://doi.org/10.1103/PhysRevB.107.035149

References 4 / 4

[8] Two distinct charge density waves in the quasi-one-dimensional metal $Sr_{0.95}NbO_{3.37}$ revealed by resonant soft X-ray scattering

Angga Dito Fauzi, Caozheng Diao, Thomas J. Whitcher, Frank Lichtenberg, Ping Yang, Mark B. H. Breese, and Andrivo Rusydi

NPG Asia Materials 16 (2024) article number 27 (1 – 13)

https://doi.org/10.1038/s41427-024-00547-7